AgriEngineering

MDPI

Article

Jasmine Flower Color Degradation User-Coded Computer Vision Image Analysis Tool and Kinetics Modeling

Humeera Tazeen [1], Astina Joice [1], Talha Tufaique [1], C. Igathinathane [1,*], Ademola Ajayi-Banji [1], Zhao Zhang [2], Craig W. Whippo [3], Drew A. Scott [3], John R. Hendrickson [3], David W. Archer [3], Lestero O. Pordesimo [4] and Shahab Sokhansanj [5]

[1] Department of Agricultural and Biosystems Engineering, North Dakota State University, Fargo, ND 58102, USA; humeera.tazeen@ndsu.edu (H.T.); astina.joice@ndsu.edu (A.J.); talha.tufaique@ndsu.edu (T.T.); ademola.ajayibanji@ndsu.edu (A.A.-B.)
[2] Key Laboratory of Smart Agriculture System Integration, Ministry of Education, China Agricultural University, Beijing 100083, China; zhaozhangcau@cau.edu.cn
[3] Northern Great Plains Research Laboratory, USDA-ARS, Mandan, ND 58554, USA; craig.whippo@usda.gov (C.W.W.); drew.scott@usda.gov (D.A.S.); john.hendrickson@usda.gov (J.R.H.); david.archer@usda.gov (D.W.A.)
[4] USDA-ARS Center for Grain and Animal Health Research, Stored Product Insect and Engineering Research Unit, 1515 College Ave., Manhattan, KS 66502, USA; lester.pordesimo@usda.gov
[5] Department of Chemical and Biological Engineering, University of British Columbia, 2360 East Mall, Vancouver, BC V6T 1Z3, Canada; shahab.sokhansanj@ubc.ca
* Correspondence: igathinathane.cannayen@ndsu.edu; Tel.: +1-701-667-3011

Abstract: Jasmine (*Jasminum sambac* (L.) Ait.) flowers, valued for their fragrance and essential oils, are extensively used in the flavor, cosmetics, and pharmaceutical industries. However, their useful life is short due to rapid color degradation and browning caused by photo-oxidative stress induced by environmental factors like light, temperature, and humidity. Therefore, the significant reduction in the visual appeal, quality, and economic value necessitates the measurement of temporal color degradation to evaluate the shelf life for jasmine flowers. A developed open-source ImageJ plugin program quantified the color degradation of jasmine petals and pedicles over 25 h. Petal area (>19 mm^2) cutoff separated the pedicles. Color degradation kinetics models, including zeroth-order, first-order, exponential decay, Page, and Peleg, using several color indices, were developed, and their performances were evaluated. VEG, hue, chroma, COM, and CIVE color indices were found suitable for kinetics modeling. Peleg and Page models ($R^2 \geq 0.99$) are suitable for petals and pedicles, respectively. Jasmine petals retained their color integrity for longer periods than pedicles. This study underscores the potential of computer vision analysis and kinetic modeling for evaluating flower quality after harvest. The color degradation dynamics were accurately characterized by the kinetic models, which provide actionable insights for optimizing storage and handling practices.

Keywords: color kinetics; flower quality; ImageJ; image processing; shelf life

check for updates

Academic Editors: Thuseethan Selvarajah and Yakub Sebastian

Received: 29 April 2025
Revised: 30 May 2025
Accepted: 12 June 2025
Published: 16 June 2025

Citation: Tazeen, H.; Joice, A.; Tufaique, T.; Igathinathane, C.; Ajayi-Banji, A; Zhang, Z.; Whippo, C.W.; Scott. D.A.; Hendrickson, J.R.; Archer, D.W.; et al. Jasmine Flower Color Degradation User-Coded Computer Vision Image Analysis Tool and Kinetics Modeling. *AgriEngineering* **2025**, *7*, 193. https://doi.org/10.3390/agriengineering7060193

Copyright: © 2025 by the authors. Licensee MDPI, Basel, Switzerland. This article is an open access article distributed under the terms and conditions of the Creative Commons Attribution (CC BY) license (https://creativecommons.org/licenses/by/4.0/).

1. Introduction

Jasmine (*Jasminum sambac* (L.) Ait.), a renowned ornamental crop, gets its name from the Persian word 'yasmin,' meaning 'gift from God' [1]. Jasmine flowers belong to the family Oleaceae and are cultivated primarily in warm and tropical regions such as South Asia and Africa. Their distinctive and delightful fragrant aroma plays a significant role in various industries, including flavor, medicine, and perfumery. Jasmine essence is extracted in the form of 'concrete' (the term used for a waxy solid extract from flowers)

or 'absolute' (the term used to represent the purified form of oil obtained from concrete after the removal of wax and other unwanted compounds) essential oil for the cosmetic or perfume industry [2–5].

There are about 200 species of jasmine flowers identified so far, 80 of which are cultivated in India, and 20 species hailing from southern India that are grown as shrubs and climbers [6]. India is the largest exporter of jasmine flowers to countries like Sri Lanka, Singapore, Malaysia, the Gulf, the UK, USA, and Canada, contributing to an INR 20 crore worth economy with a production area of 8000 ha [1]. Among the many varieties, *J. sambac* (Arabian/Tuscan jasmine), *J. auriculatum*, and *J. grandiflorum* (Royal/Spanish jasmine) are commercially cultivated [7]. For the general public and other vendors' consumption, fresh jasmine flowers are sold in local flower markets (Figure 1). Jasmine flowers are utilized for various occasions, including religious activities, ceremonies, and in decorations, such as garlands, loose flowers, or assembled into strings using cotton thread (Figure 1), enhancing both beauty and aroma [8]. To ensure the highest quality of flowers, skilled and experienced manpower is employed to handpick jasmine petals from dawn to early morning hours for better handling and freshness retention [9].



Figure 1. Jasmine flower trade and usage: (**a**) fresh jasmine flowers of Sambac variety sold in flower markets by weight and (**b**) assembled strings ready for wear and other decorative use (source: www.indiamart.com/proddetail/fresh-jasmine-flower-10391290248.html accessed on 13 June 2025).

The postharvest care of cut flowers can increase the value of jasmine flowers by 5–10 times that during cultivation [7]. Hence, postharvest management is necessary for extending the shelf life of the flowers. Improper handling, packaging, and storage contribute to approximately 20–40% of postharvest losses of flowers [6]. The fragrance of the jasmine flowers is attributed to their level of maturity and freshness, and one of the major obstacles in preserving the freshness of the flowers is their rapid degradation [10].

Furthermore, the postharvest life of jasmine flowers is substantially constrained by various factors, including illumination, thermal conditions, and humidity levels, which precipitate photo-oxidative stress, pigment disintegration, and moisture loss [9]. This phenomenon results in petal browning and considerable degradation of color, thus adversely affecting the aesthetic appeal, overall quality, and commercial value of jasmine flowers. Warmer temperatures facilitate flower blooming, hastening the release of the characteristic fragrance from the flowers and leading to the browning of petals [11]. Conventional techniques for precisely assessing temporal color variations and quantifying postharvest color deterioration are often deemed impractical. Because of these limitations, there exists a critical need to develop a robust, automated methodology for measuring the color change,

evaluating, and designing methodologies during the process of packaging and storage that help retain the freshness of jasmine flowers.

In recent years, non-destructive techniques such as computer vision and digital image analysis have been increasingly adopted for assessing postharvest quality in perishable horticultural commodities [12]. Computer vision enables the acquisition and processing of digital images to extract quantifiable parameters, such as color, shape, and size, offering non-destructive, efficient, and repeatable methods for quality assessment [13]. This approach has been successfully applied in agriculture, including color calibration, dimensional analysis of floral parts, and classification of agricultural products based on physical traits [14]. These methods offer substantial advantages over traditional techniques by enabling objective, repeatable, and high-throughput monitoring of visual and physical attributes [15–17].

Several studies highlight the effectiveness of these techniques in diverse contexts. In the domain of color kinetics studies, color change is commonly used as an indicator of senescence and quality degradation, especially in floral and leafy produce. Kinetics modeling was conducted to monitor the degradation of color in saffron flowers during thin-layer drying [18]; to analyze the kinetic decay of anthocyanins in purple sweet potatoes under thermal treatment [19]; to study the effect of storage temperature on rose petal color stability [15]; to assess discoloration kinetics in pear slices using colorimetric indices derived from digital images [20]; and to track chlorophyll degradation in leafy greens utilizing hyperspectral imaging [21]. These studies demonstrate the potential of digital imaging and analysis in overcoming the limitations of conventional methods, providing a reliable platform to monitor subtle changes, such as petal and pedicle browning in jasmine flowers over time, influenced by general postharvest storage conditions.

However, most of the existing research has focused on either food crops or ornamental flowers subjected to drying or thermal stress, with limited work exploring passive degradation (i.e., natural senescence) under ambient postharvest conditions. Despite the substantial commercial importance of jasmine flowers in South and Southeast Asia, particularly for religious, aromatic, and cosmetic uses, systematic investigations into their postharvest color dynamics are limited. Currently, there is no field-deployable tool available for quantifying the kinetics of jasmine color degradation developed using an open-source platform. Furthermore, a comprehensive comparison of color kinetic models has not been conducted for this specific application.

ImageJ, (version 1.54p) an open-source image analysis platform developed by the National Institutes of Health (NIH), has become a powerful and accessible tool for implementing various computer vision methods [22]. Its extensibility, through plug-ins and macros, allows for customized image analysis workflows suited to diverse research needs, including those in agricultural and postharvest studies. It was used to develop user-coded tools to evaluate floral dimensions of sunflowers, color calibration, plant stand count, and soybean phenology [14].

By combining accessible imaging tools with robust statistical modeling, this study addresses the aforementioned research gaps by presenting a novel, ImageJ user-coded plugin capable of automating the quantification of color degradation in jasmine flowers. The plugin operates on temporal digital images obtained under standardized imaging conditions, extracts multiple color indices (e.g., VEG, ExG, hue, chroma), and treats flower structures (petals and pedicles) as distinct components for analysis. It seamlessly integrates with R-based modeling pipelines to fit various kinetic models, including zeroth-order, first-order, Page, and Peleg, to time-series color data. This approach enables rigorous, quantitative assessment of floral senescence under ambient conditions without the necessity of expensive hardware or proprietary analysis platforms.

Given the capability and various applications of ImageJ, in conjunction with digital imaging, it is possible to develop standardized protocols for monitoring color deterioration

in jasmine petals, enabling objective quality assessment and supporting the development of optimized postharvest management strategies. This integration holds the potential to reduce losses and improve the marketability of jasmine flowers significantly. Therefore, the overall objectives of this research are to (i) develop a methodology to capture images of jasmine flowers and separate the bud and pedicle components for further analysis, (ii) evaluate the dimensional characteristics of jasmine petal and pedicle components, (iii) develop an ImageJ computer vision plugin for analyzing the color of flower components, and (iv) build color degradation kinetics models for jasmine flower components.

2. Materials and Methods

2.1. Overall Workflow of the Study Analysis

The workflow followed in this research is presented in the flowchart in Figure 2. It is essential to capture the digital image of the flowers in a consistent manner so that the dimensional color characteristics can be assessed across the time of the experiment. The images are then loaded into ImageJ and preprocessed for subsequent analysis processes. A computer vision plugin was developed with user-developed functions and application programming interfaces (APIs). This plugin was executed within the ImageJ environment, enabling automated processing and analysis of image datasets. The plugin facilitates a comprehensive evaluation of the jasmine flower color properties of the petals and pedicles separately. Standard ImageJ outputs, coded in the plugin, also evaluate the dimensional characteristics of the flower components at different time steps. The generated data from the plugin can be saved as a CSV worksheet for easy data exchange. The extracted color data are finally processed in the R programming language to develop the color degradation kinetics model and its visualization. This framework enables precise quantification of the postharvest senescence patterns in jasmine petals and pedicles. The various activities are subsequently described in detail.

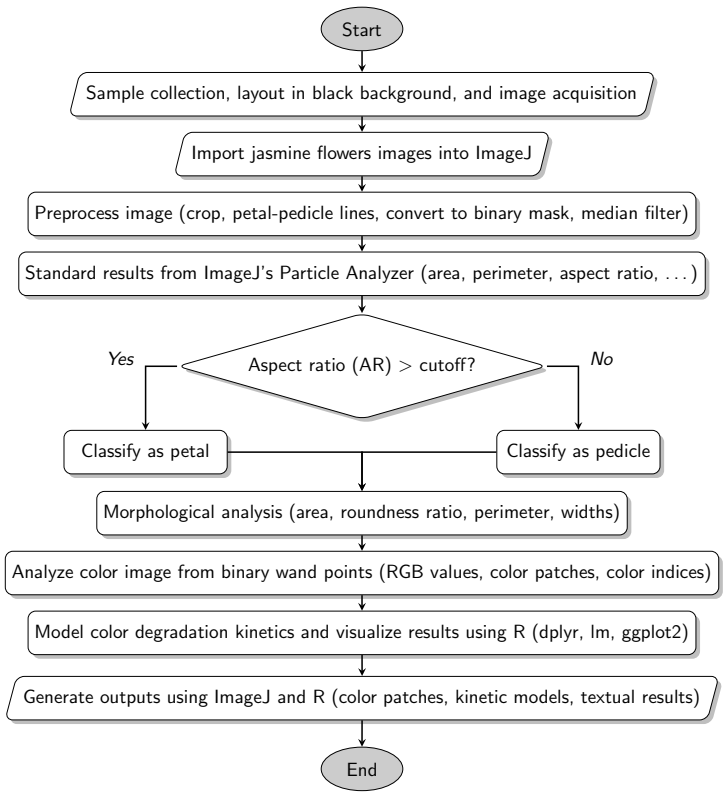


Figure 2. Overall process workflow of jasmine flower component color degradation kinetics and dimensional characteristics study.

2.2. Sample Collection and Experimental Setup

Jasmine flowers of Sambac variety (Figure 1) were procured from a single batch at a local flower market in the Tirunelveli District of Tamil Nadu, India. All flowers were from the same vendor and were presumed to belong to the same cultivar and from the same field of production based on morphological traits. To retain their freshness, the flowers were wrapped in a damp cloth to prevent early dehydration, which is the common local preservation practice, and stored until they were used for image capture and further analysis. Although this procedure minimizes intra-sample variability, it limits the broader applicability of findings across subspecies or different jasmine cultivars.

The images were acquired in a controlled condition designed to minimize ambient lighting interference. The setup consisted of a dark room maintained at 70 °F with no ventilation. A white LED light panel (11 in diameter, maximum wattage of 13 W, 110 V, daylight setting with 5000 K color temperature, and 1000 lx) was positioned 30 cm directly above the layout of flowers to provide uniform illumination, minimizing shadows or reflections. An Apple iPad (9.7 in 6th generation) with a high-resolution (8 MP) camera was mounted vertically on a tripod at a fixed height and orientation. Manual exposure settings were applied to all images to avoid the auto-adjustment effects. The flowers were arranged on a black A4 sheet (210 mm × 297 mm) with corner markers utilized for subsequent subsample extraction (Figure 3). Images were captured hourly for a total of 25 h without disrupting the layout of flowers. The combination of the multi-source LED light panel and the black background effectively reduced or concealed the shadows cast by individual flowers, resulting in crisp images with distinct flower outlines that facilitate efficient image processing (Figure 3).

The flowers were evenly divided into four quadrants. Approximately 35–40 flowers were placed in each quadrant, and the flowers in each quadrant were considered four distinct samples. Markers on each corner of the image subsamples (total 16) were arranged, which is helpful for cropping the subsamples during analysis (Figure 3). This entire arrangement is left undisturbed during the whole experiment, and images were captured at regular 1 h intervals.

After loading the image in ImageJ and using the rectangle selection tool and noting the pixel dimensions of the entire image against the dimensions of the A4 sheet, the resolution of the image was obtained as 225 DPI (dots per inch). This DPI value was applied to the other dimension results derived in pixels to obtain the physical dimensions in mm as

$$d_{\text{physical}} = d_{\text{pixel}} \times 25.4/225 \quad (1)$$

where d_{physical} is the linear dimension in physical units of mm, d_{pixel} is the linear dimension in the image in pixel units, 25.4 is the unit conversion factor from inch to mm, and 225 is the constant DPI of the acquired image.

2.3. Image Acquisition of Jasmine Flowers and Subsample Image Creation

An Apple iPad with a high-resolution camera (iPad: 9.7 in 6th generation; Camera: 31 mm wide, f/2.4 aperture, 8 MP, ISO: 320) fitted on a tripod and mounted vertically was used to capture the images. Necessary adjustments were made in the camera settings to capture good-quality images at hourly intervals until the flowers were completely dried and changed to a dark and stable color. Each image was captured by maintaining the same height of 30 cm consistently throughout the experiment (Figure 3).

Subsample images were created by cropping the original image with the markers (Figure 3) as guides. The subsample images can be created in ImageJ after loading the original image and using its tools. The 'Rectangle' selection tool was used to delineate subsamples, with the markers guiding the process, and the 'Crop' tool command generated

the subsample images and was saved under identifiable names. It is often convenient to duplicate the original image ('Duplicate' command) four times for the four samples. The rectangle region of interest (ROI) used was applied to the next image ('Restore Selection' command) and adjusted, when needed, to create the next sample.

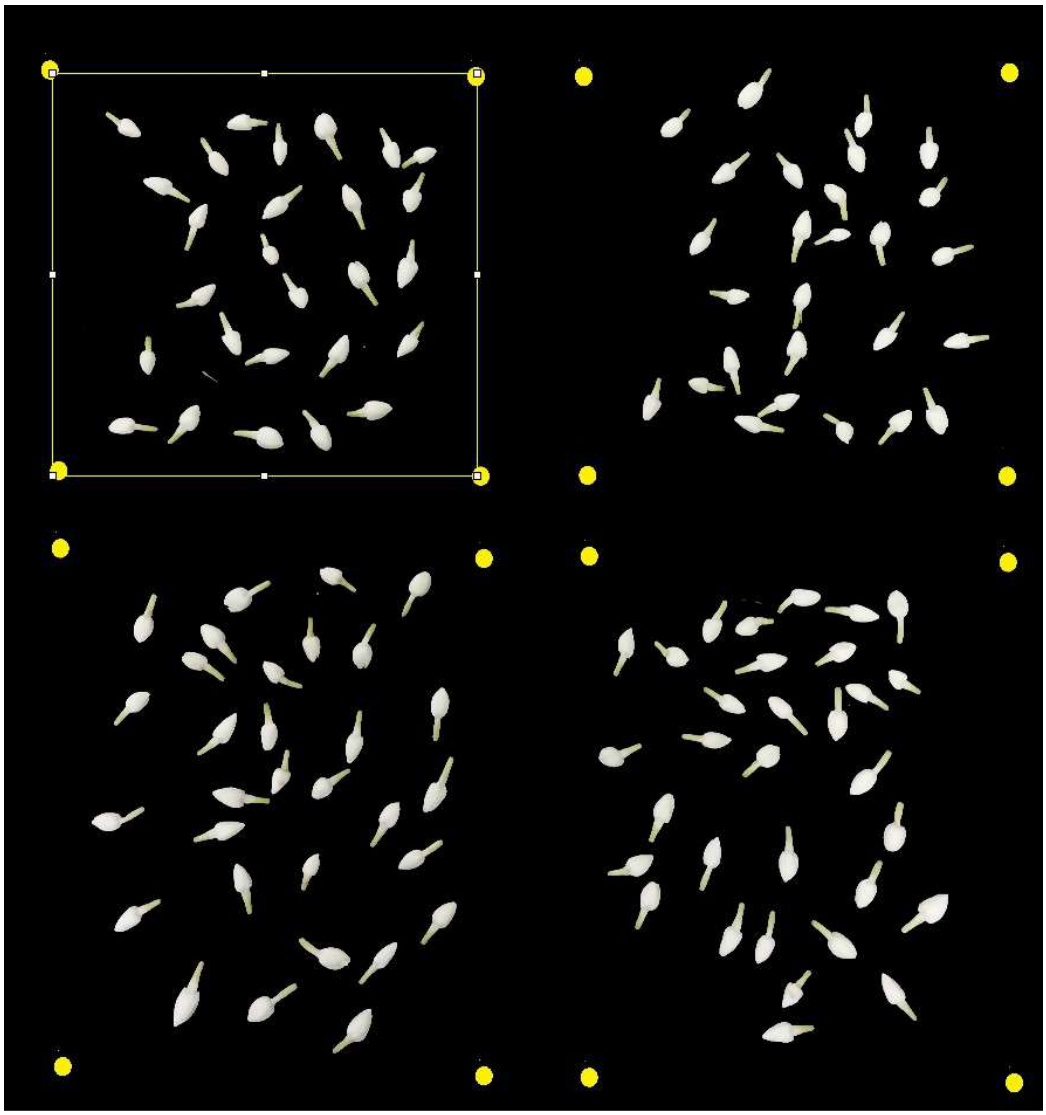
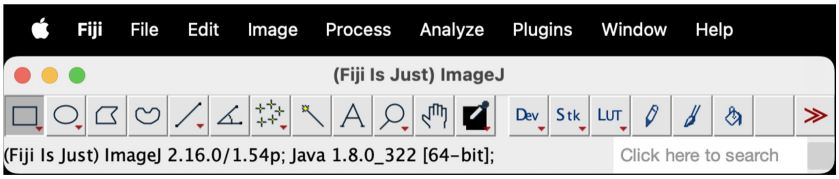


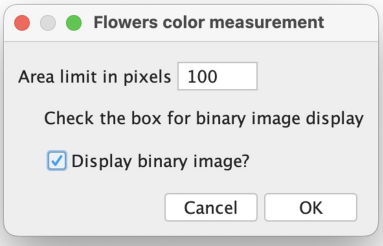
Figure 3. Jasmine flower fixed layout image showing samples arranged in four different quadrants on a black A4 sheet for image acquisition (210 mm × 297 mm; DPI = 225). The markers arranged at the four corners of the sample are for generating subsamples by drawing ROIs, as shown, for each quadrant and subsample images obtained by cropping.

2.4. Plugin Development for Jasmine Flower Components, Color Patch, and Dimensional Characteristics

Images of jasmine flowers were imported into Fiji, an advanced IDE of ImageJ. The plugin was coded in the Java language using the Fiji IDE, which provides various helpful features for code development (Figure 4a). The plugin front panel reads the 'Area limit in pixels' to filter out small objects and dust particles, and the 'Display binary image?' checkbox to visualize the binary images (Figure 4b). The plugin generates the color patches and RGB values for analysis. Several methods were created to achieve specific tasks and were called into the main method to achieve the results.



(a) Fiji – ImageJ software



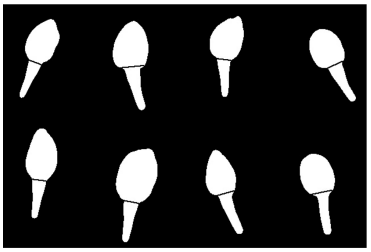
(b) Front panel of the developed plugin



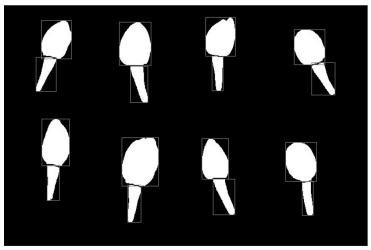
(c) Original jasmine samples



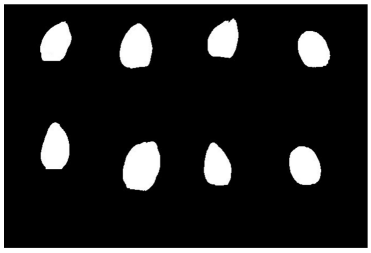
(d) Manually segmented jasmine flowers



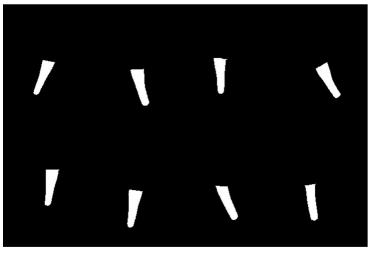
(e) Processed binary image mask



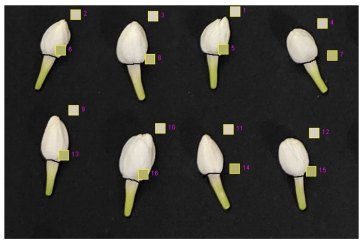
(f) Boundary box of processed binary image



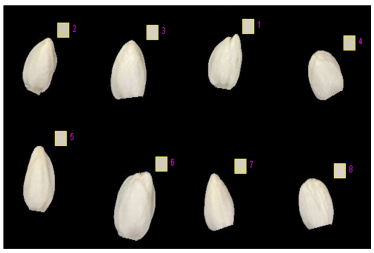
(g) Extracted binary jasmine petals image



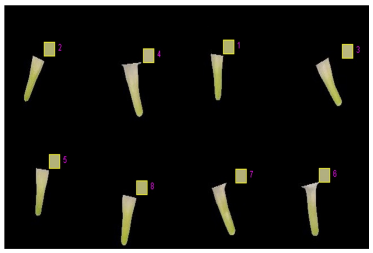
(h) Extracted binary jasmine pedicles image



(i) Measured color of whole flowers



(j) Measured color of jasmine petals



(k) Measured color of jasmine pedicles

Figure 4. ImageJ (Fiji) image analysis system, developed plugin front panel, and the process of generating jasmine flower components and evaluating their color patches with numbered labels.

2.4.1. Petal and Pedicle Segmentation

It was necessary to separate the petals from the pedicles of the jasmine flowers digitally for the color analysis because (i) these components are predominantly of different colors (petals are white and pedicles are green) and thus a simple average color of the whole flower is not representative and useful for the analysis, and (ii) the petals are a significant component of economic importance and their color is the indicator of quality and market value, hence needing to be evaluated as a separate component. An illustration of the original jasmine flower image sample and the manually segmented petals and pedicles are shown in Figure 4c and Figure 4d, respectively.

To achieve this separation from the original image (Figure 4c), in the subsample color images, a 2-pixel black line was drawn using ImageJ's 'Pencil Tool,' where the width was assigned as 2 pixels (Figure 4d). This 2-pixel width is the minimum line thickness that makes a clear separation of components, and it represents only about 1.33% of the average length of the whole flower. It should be noted that a single-pixel line does not separate components, as components are connected along the perpendicular direction when two black pixels touch on their vertices, which is drawn by a 1-pixel width line. Once these segmentation lines are drawn in the color images, they are carried through the entire process, and the flower components stay separate. It is possible to develop advanced algorithms to automate the segmentation of the petals and pedicles, and this should be looked into in future research.

2.4.2. Binary Image Creation

The manually segmented color images (Figure 4d) were converted to a binary image mask (Figure 4e) for further analysis. The actual sequence of operations that created the binary masks are as follows: (i) duplication of the image using the 'Duplicate' command, (ii) creation of the grayscale image using the '8-bit' command, (iii) generation of the corresponding binary image mask using the 'Convert to Mask' command, and (iv) removal of small particles and opening divides using the 'Open' command. The binary image containing two values, 0 for black and 255 for white pixels, was efficient for analysis and mathematical calculations.

2.4.3. Particle Analysis and Dimensional Characteristics

The binary image (Figure 4e) was the input to the particle analysis routine. The necessary measurements, such as area, centroid, perimeter, bounding rectangle, shape descriptor, and Feret's diameter, were set through 'Set Measurements.' The 'ParticleAnalyzer' class was used to execute the selected measurements and options of the 'Analyze Particles' command (e.g., display results, exclude on edges, include holes) and generate the results in the form of 'ResultsTable.'

For all the particles (petals, pedicles, and whole flowers—dimension variation), the analyzed results include area, centroid coordinates (x_c, y_c), bounding rectangle (Figure 4f) information (ROI_x, ROI_y, ROI_{width}, and ROI_{height}), shape descriptors (aspect ratio, circularity, and roundness), and Feret diameter, which is the maximum dimension of the particle that is equal to the circumscribed circle. The units of these measurements are pixels and can be converted into physical units (e.g., mm) using the DPI value (225) of the images.

2.4.4. Petal and Pedicle Separation from Jasmine Images

With the manual segmentation, the particle analysis routine generated the various dimensional measurements (Section 2.4.3), and from those results, it was possible to automatically identify, separate, and group the petals from the pedicles for individual component analysis. As the area of petals is greater than that of pedicles (Figure 4g,h), the area

served as a distinguishing factor between petals and pedicles. Additional factors, such as perimeter, aspect ratio, and roundness, could also work and could be used when there is a tie.

2.4.5. Color Analysis and *Lab* Value Generation

The mean colors of the jasmine flower petals and pedicles were calculated from the original and binary images. With the binary image and 'Wand.autoOutline(x_c, y_c),' the boundary of the object was obtained and the coordinates of the polygon ROI were generated for pixel-color extraction. For the average color calculation, the bounding rectangle ROI of each object in the binary image was taken in order, and a double nested loop traversal was conducted starting from coordinates ROI_x and ROI_y across ROI_{width} and down ROI_{height}. This traverse was checked to see whether the active pixel '(u, v)' was inside the wand polygon ROI using the 'PolygonRoi.contains(u, v)' command. When the active pixel is inside with reference to *binary image*, then the *R*, *G*, and *B* color values of the pixel are extracted from the same location on the original *color image* and added to the respective Apache Commons Math Tool's 'DescriptiveStatistics' class object. After the completion of traversal, the mean color values (R_{mean}, G_{mean}, and B_{mean}) and standard deviation (STD) values can be easily obtained from these objects using appropriate methods. The mean color channel values are stored in arrays for later use, and the 'DescriptiveStatistics' objects are reset for the next object in the image. The dataset (time-series RGB values of petels and pedicles) used in the study is available from DOI: https://doi.org/10.17632/42p3sxt73r.1.

The mean *R*, *G*, and *B* color values of jasmine flower components were converted to CIELAB (International Commission on Illumination) *Lab* color space using the function 'RGBtoLAB()' from the 'ColorSpaceConverter()' class object. This color space describes all colors visible to the human eye in three values: *L* = lightness, *a* = green–red opponent colors, and *b* = blue–yellow opponent colors (these variables are also generally represented as L*, a*, and b*, but in this study we consistently use *L*, *a*, and *b*). The *L*, *a*, and *b* values were stored in corresponding arrays for individual objects in the image, and these values, as well as *R*, *G*, and *B*, were used in the calculation of color indices that were used in kinetics modeling.

2.4.6. Color Patch Visualization with Labels

The overall color of the jasmine flower and its components are visualized through color patches, which are small rectangles (20-pixel side) drawn at the top right corner of the object filled with a color derived from the mean *R*, *G*, and *B* color values (Section 2.4.5). Initially, a duplicate of the segmented original color image was duplicated, and the color patches were drawn on that, leaving the original image undisturbed. The top-right corner of the object was obtained from the ROI coordinates. This was used to coincide with the bottom-left corner of the color patch (Figure 4i). The 'ImageProcessor.setColor()' was set to the derived mean *RGB* values, and 'ImageProcessor.fillRect()' with ROI parameters drew the color patch and filled with the mean color of the object as input.

It was convenient to separate the petals and pedicles into different groups, apply the color patches for visualization, and use the collective data for the color degradation kinetics modeling (Figure 4j,k). Furthermore, to identify the objects, a label was drawn on the right side of the color patch, where the label numbering scheme follows top-to-bottom and left-to-right ordering using the 'ImageProcessor.drawString()' command.

2.5. Color Degradation Kinetics Modeling

2.5.1. Common Kinetics Models for Color Degradation and Their Characteristics

In postharvest research, color degradation is often modeled using empirical or semi-empirical kinetic equations to quantify changes over time and forecast shelf life. These

models help characterize the dynamics of pigment loss and facilitate quality control decisions for perishable products. The most widely employed models include zeroth-order, first-order, exponential decay, Page, and Peleg, each exhibiting distinct mathematical structures and suitability depending on the material behavior and degradation mechanism, including changes in biological material [23–27], and their Equations (2)–(6) are presented in Table 1.

Table 1. Common kinetic models employed in the present study to analyze the color degradation of jasmine flower components.

Model	Equation	Eqn. Number	References
Zeroth-order kinetic model	$C = C_0 + k_0 t$	(2)	[20,27,28]
First-order kinetic model	$C = C_0 \exp(k_0 t)$	(3)	[19,20,28,29]
Exponential model	$C = \exp(-k_0 t)$	(4)	[26,30]
Page model	$C = \exp(-k_0 t^n)$	(5)	[18,26,27]
Peleg model	$C = C_0 + \frac{t}{k_0 + k_1}$	(6)	[26,27]

C and C_0 are the initial and final color values of each color index, respectively. t is time in hours, and k_0, k_1, and n are the corresponding kinetics model constants.

The general characteristics of each kinetic model when applied to a hypothetical color degradation are illustrated in Figure 5. For the purpose of visualizing the trends of these kinetic models (Table 1), some arbitrary constants were selected. The constants used for each model are $C_0 = 100$ and $k_0 = -5$ for zeroth order; $C_0 = 100$ and $k_0 = -0.3$ for first order; $k_0 = -0.3$ for exponential; $k_0 = 0.3$ and $n = 1$ for Page; and $C_0 = 100$, $k_0 = 2$, and $k_1 = 10$ for Peleg.

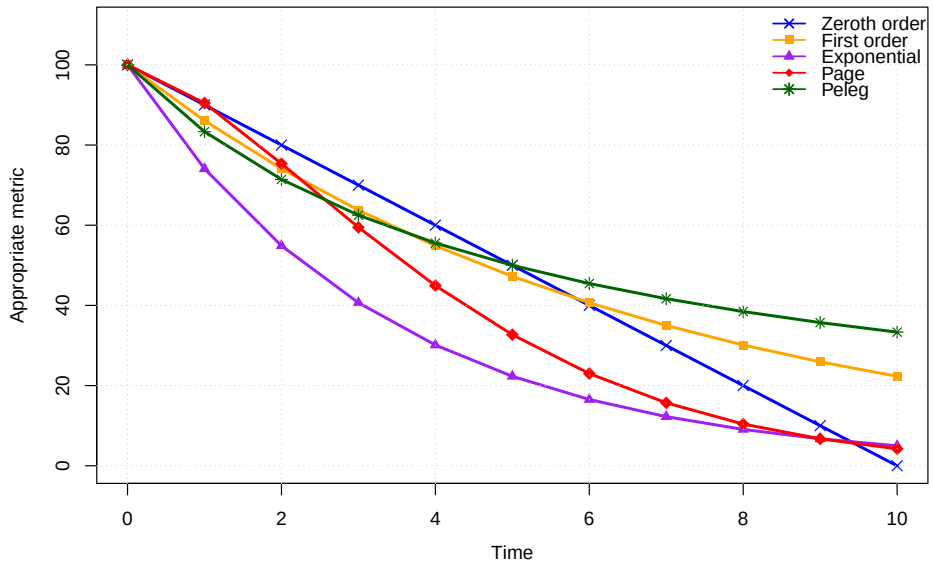


Figure 5. General characteristics of the selected kinetic model for color degradation with arbitrary constants showing the model trends.

The zeroth-order model assumes a constant rate of color loss, independent of concentration, and is typically used when degradation occurs due to constant external factors. The first-order model, by contrast, assumes a rate proportional to the remaining color intensity and is suitable for processes involving oxidative or enzymatic breakdown [31]. The exponential decay model is used to capture monotonic decline where no asymptote is evident. More advanced empirical models have emerged to better fit non-linear and time-dependent changes. The Page model, initially developed for drying kinetics, introduces a power-law term to adjust the shape of the decay curve, making it particularly

effective for biological materials that exhibit fast initial degradation followed by slower decline. The Peleg model, originally proposed for moisture sorption kinetics, includes two adjustable parameters and does not assume an exponential form, offering flexibility in describing complex degradation behaviors [32,33].

While previous studies have applied kinetic models to color degradation in foods or dried plant products, there is a lack of research applying a comprehensive kinetic modeling framework to floral senescence, particularly using image-derived indices (Table 2). Therefore, this study applying these color indices for modeling the color degradation kinetics for jasmine flower components is a unique contribution. The comparative trend analysis followed in the study validates the importance of evaluating multiple models to determine the most appropriate one for specific flower components and color indices.

Table 2. Color indices used for color degradation kinetics of jasmine flower components.

Color Index	Equation	Eqn. Number	Reference
Total color difference (ΔE)	$\Delta E = \sqrt{(\Delta L)^2 + (\Delta a)^2 + (\Delta b)^2}$	(7)	[19,20,34]
Hue (hue)	$Hue = \sqrt{a^2 + b^2}$	(8)	[20,21,35]
Chroma (Ch)	$Ch = \tan^{-1}\left(\frac{b}{a}\right)$	(9)	[35]
Browning index (BI)	$BI = \frac{100\,(x-0.31)}{0.17}$; where, $x = \frac{a+1.75\,L}{5.65\,L+a-3.01\,b}$	(10)	[19,36]
Color index vegetation (CIVE)	$CIVE = 0.44\,R - 0.88\,G + 0.38\,B + 18.78$	(11)	[27]
Vegetative (VEG)	$VEG = \frac{G}{R^{0.67}.B^{0.33}}$	(12)	[27]
Excess green (ExG)	$ExG = 2\,G - R - B$	(13)	[26]
Excess green–red (ExGR)	$ExGR = ExG - (1.4\,R - G)$	(14)	[14]
Combination (COM)	$COM = 0.25\,ExG + 0.3\,ExGR + 0.33\,CIVE + 0.12\,VEG$	(15)	[14]
Whiteness (WI)	$WI = \frac{B}{\max(B)} \times 100$	(16)	[36]
ISO brightness (ISO_B)	$ISO_B = \frac{R+G+B}{3}$	(17)	[36]
Hunter whiteness (Hunter_WI)	$Hunter_WI = \frac{b-a}{b+a} \times 100$	(18)	[36]

Color values: R = red; G = green; B = blue; L = lightness; a = redness or greenness; and b = yellowness or blueness.

2.5.2. Color Vegetation Index Calculation

The RGB and *Lab* values were used to calculate various color indices treated as independent variables in the color degradation models and to evaluate their performance in modeling (Equations (7)–(18); Table 2).

These color indices are widely used in plant science, food quality, and postharvest studies to quantify visual attributes, such as greenness, browning, lightness, and chromaticity. Indices like ExG, VEG, and CIVE are particularly sensitive to chlorophyll-related greenness and are commonly employed in vegetation health monitoring [37]. In contrast, total color difference (ΔE), hue, and chroma provide a perceptual measure of overall color change [35]. The browning index (BI), ISO brightness, and whiteness-related measures (WI, ISO_B, Hunter_WI) are useful in detecting tissue degradation, loss of freshness, or enzymatic browning, all of which are critical in postharvest floral studies [38,39].

These indices were selected not only for their proven sensitivity to changes in pigmentation but also for their computational simplicity and compatibility with image-derived color channels. Each index (Table 2) was treated as a potential predictor of color degradation, and its performance was later evaluated through kinetic modeling. The combination of multiple indices allows for a robust, multidimensional characterization of color loss across different floral components (petals and pedicles), enhancing both modeling accuracy and interpretability. The dataset also contains the consolidated RGB values and the derived color indices used for the kinetics modeling (DOI: https://doi.org/10.17632/42p3sxt73r.1).

2.5.3. Color Kinetics Modeling, Data Analysis, and Visualization Using R Program

The color degradation data were fitted to various kinetic models using R statistical software (version 4.4.2) through linear and nonlinear models. For fitting the kinetic models, the following steps were performed in 'R,' starting with installing and loading libraries like 'readxl,' 'ggplot2,' 'minipack.lm,' 'qpcR,' and 'dplyr' for data processing, visualization, and modeling. Next, a dataset with time-series metrics and color indices values was imported for analysis. A cleaner data frame was created by selecting relevant columns for modeling and defining custom functions to calculate Akaike information criteria (AIC) for model evaluation. Linear model (zeroth-order) and non-linear models (first-order, exponential decay, Page, and Peleg) were fitted by using 'nlsLM()' from the 'minipack.lm' package [40] and performance metrics like the coefficient of determination (R^2), root mean square error (RMSE), and AIC were calculated [41,42]. Finally, the data were visualized by plotting using 'ggplot2' [43] and overlaying the fitted models for comparison. Based on the statistical outputs and AIC scores, the best-fit model for each of the color indices was identified and reported. Overall results of the combination of color indices and models were also visualized using heatmaps with selected model performance metrics using 'ggplot2.'

3. Results and Discussion

3.1. Image Acquisition and Preprocessing

High- resolution digital images of a subsample of jasmine flowers captured over a 25 h period at 1 h intervals, with petals and pedicles manually segmented, are presented in Figure 6. It can be observed from the images that the simple standardized setup used in the image captures minimized variations due to ambient light and camera angle, ensuring consistent image quality and reproducibility.

From the sequence of images, the initial visual observation indicated blooming of jasmine flowers between 3 and 5 h, and a notable color change became evident from the 12th hour. The color degradation process continued until the jasmine flowers reached full natural dehydration, a process that lasted for a total of 25 h (Figure 6). The overall dimensional shrinkage of the flower components can be observed from 16 h and is evident from 21 h. Based on the variety of the jasmine flowers, the final darkened color varies (e.g., pink, brown, black).

3.2. Automatic Petals and Pedicles Segmentation

The range of area values obtained from all the samples for petals was 2156–3978 pixel^2 and for pedicles it was 557–661 pixel^2. The mean value of the area of the petals was about five times that of the pedicles. Hence, the projected area was used as the criterion to automatically distinguish jasmine petals from the pedicles. Based on Equation (1), a cutoff value of 1500 pixel^2 (for DPI = 225) or 19 mm^2 can be used as a cutoff value to identify the petals and pedicles.

3.3. Dimensions of Jasmine Flowers

The dimensional characteristics of the whole flowers, petals, and pedicles were evaluated at 1 h (start), 12 h (middle), and 24 h (end) as presented in Table 3. The physical dimensions (e.g., mm, mm^2) of the flower components were evaluated from the image pixel values using Equation (1). The average area of whole jasmine flowers increased from 35.56 mm^2 to 41.75 mm^2 after 12 h, and later decreased to 18.87 mm^2 at 24 h, confirming substantial shrinkage over time. Similar reductions were observed in perimeter (32.92 mm to 23.43 mm) and Feret diameter (13.75 mm to 7.63 mm). Although the aspect ratio remained relatively stable, the circularity and roundness (higher values represent circular shapes and lower elongated shapes) showed a modest decrease over time—indicating the

opening of petals, increasing the overall width, followed by structural compaction of flower components due to moisture loss and collapse of tissue.

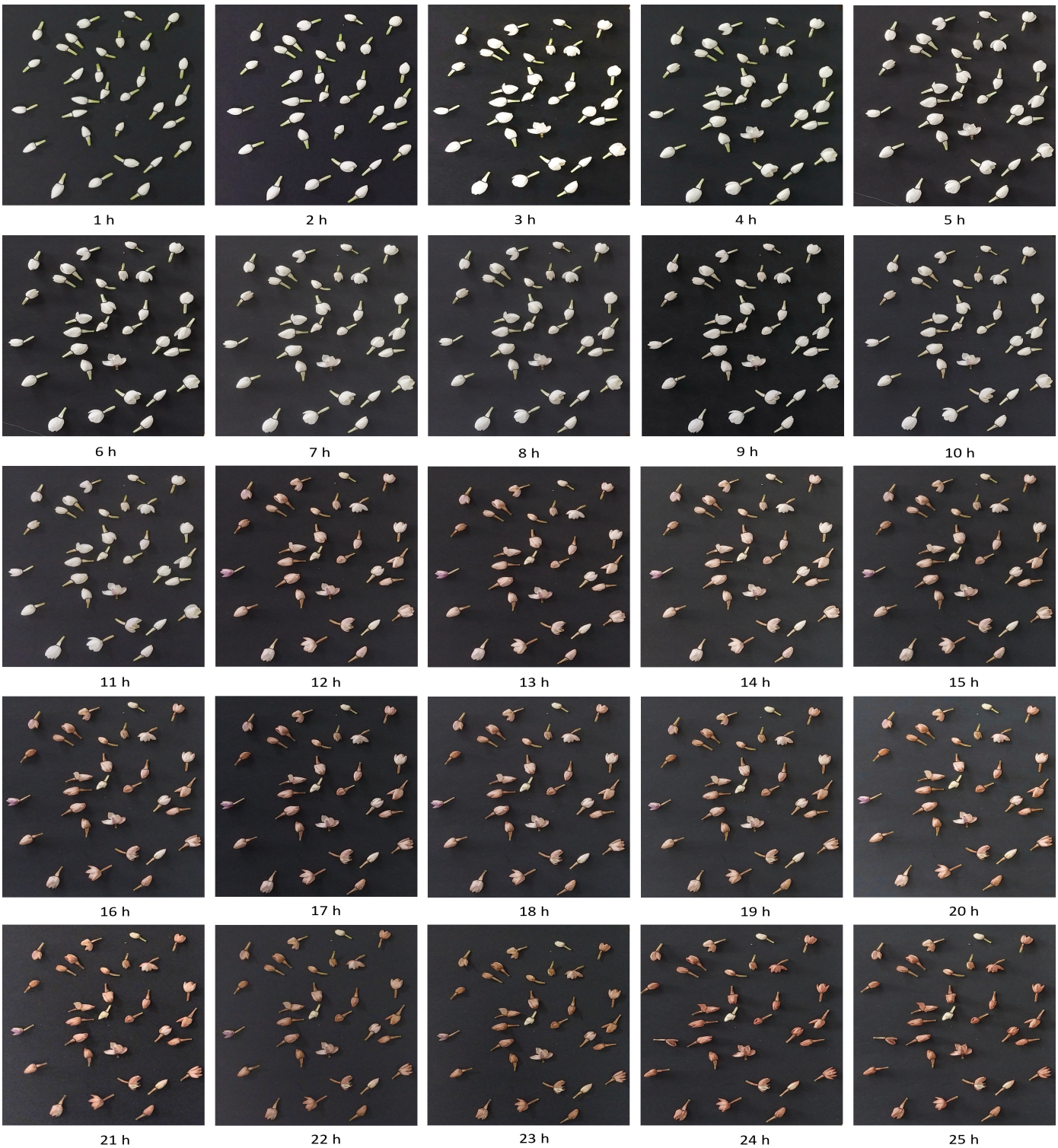


Figure 6. Image of jasmine flowers showing the effect of time on the color deterioration of the components. The images represent one of the four subsamples of the flowers manually segmented as petals and pedicles for the grouping of components for analysis.

Table 3. Dimensional characteristics of whole jasmine flowers at initial (1 h), middle (12 h), and end (24 h) of experiment.

Jasmine Flower Components	Area (mm^2)	Perimeter (mm)	Circularity	Feret (mm)	Aspect Ratio	Roundness
Whole 1 h	35.56 ± 2.06	32.92 ± 2.34	0.52 ± 0.03	13.75 ± 0.92	2.8 ± 0.05	0.57 ± 0.02
Whole 12 h	41.75 ± 2.90	30.67 ± 2.20	0.49 ± 0.05	10.8 ± 0.94	2.4 ± 0.24	0.53 ± 0.02
Whole 24 h	18.87 ± 2.02	23.43 ± 2.30	0.48 ± 0.03	7.63 ± 0.46	1.98 ± 0.15	0.37 ± 0.02
Petals 1 h	30.53 ± 7.37	32.93 ± 10.71	0.78 ± 0.08	8.97 ± 1.91	1.68 ± 0.48	0.74 ± 0.11
Petals 12 h	39.62 ± 14.59	28.05 ± 8.01	0.66 ± 0.14	8.59 ± 1.82	1.49 ± 0.29	0.69 ± 0.13
Petals 24 h	30.65 ± 10.41	22.09 ± 2.57	0.41 ± 0.18	8.18 ± 1.03	1.39 ± 0.22	0.63 ± 0.12
Pedicles 1 h	9.42 ± 2.09	14.7 ± 2.57	0.62 ± 0.31	5.93 ± 1.07	3.68 ± 1.59	0.49 ± 0.32
Pedicles 12 h	5.29 ± 3.26	11.95 ± 6.03	0.55 ± 0.08	4.86 ± 2.46	3.2 ± 1.94	0.37 ± 0.24
Pedicles 24 h	3.82 ± 3.77	9.34 ± 7.79	0.51 ± 0.24	3.71 ± 3.01	3.08 ± 0.55	0.34 ± 0.07

Values represent the mean ± the standard deviation of the four subsamples.

The dimensional characteristics of petals showed a distinct pattern (Table 3). Similar to whole flowers, bud area increased from 30.53 mm^2 at 1 h to 39.62 mm^2 at 12 h, suggesting petal expansion and flower blooming during the early hours of postharvest, which was followed by a decline to 30.65 mm^2 by 24 h, indicating the onset of tissue dehydration. A decreasing trend was observed in feret diameter (8.97 mm to 8.18 mm) and perimeter values (32.93 mm to 22.09 mm) over a period of 24 h. Circularity and roundness declined throughout the drying process, reflecting progressive blooming of the petals and moving away from the round shape of buds.

In contrast, the pedicles exhibited a steady decline in all dimensional attributes across the three time points. The area reduced from 9.42 mm^2 to 3.82 mm^2 (Table 3), while the perimeter dropped from 14.7 mm to 9.34 mm. It was also noted that the aspect ratio decreased from 3.68 to 3.08, indicating consistent shrinkage and change in the length and width of the pedicles. Notably, circularity and roundness values decreased with time, suggesting pedicle tissues curled and compacted during the dehydration process, in line with their physiological structure and function during the period of 24 h. These dimensional analyses validated the progression of senescence and set the stage for subsequent color degradation modeling [44–46].

3.4. Color Degradation Analysis

The temporal color degradation of jasmine flowers kept at room temperature was assessed using 12 distinct color indices (ΔE, CIVE, VEG, ExG, ExGR, COM, BI, WI, ISO_B, Hunter_WI, hue, Ch). For both petals and pedicles of jasmine flowers, all the color indices showed a progressive decline in their values, indicating significant shifts in color as the flowers transitioned from fresh to dried conditions.

The reduction in color values can be primarily attributed to natural senescence (aging), photo-oxidative stress, moisture loss, and the degradation of pigments (chlorophyll and carotenoids), caused by prolonged exposure to ambient conditions [47]. The study reports that cut flowers can rapidly lose water through the stem, leading to wilting and color fading due to reduced turgor pressure [48]. Ethylene, a plant hormone naturally produced by flowers, accelerates senescence and color loss when present in high concentrations [49]. The browning observed during the process is likely a result of enzymatic and non-enzymatic oxidation reactions occurring in the floral tissues. Wilting and browning collectively diminish the aesthetic quality, marketability, and economic value of jasmine flowers [50–52].

When comparing the petals and pedicles, distinct differences in degradation patterns were observed. Jasmine petals exhibited higher initial color values and a slower rate of

degradation compared to the pedicles. This behavior can be attributed to their delicate structure and higher pigment concentration, which potentially provides greater resistance to environmental stress. Conversely, pedicles demonstrated a faster decline in color indices, likely due to their structural properties, lower pigment density, and greater susceptibility to oxidative and environmental stressors [51,53,54].

3.5. Kinetic Modeling of Jasmine Flower Components and Model Performance

3.5.1. Model Selection and Performance Evaluation

In this study, five kinetic models, namely zeroth-order, first-order, exponential, Page, and Peleg (Table 2), were employed to describe the color degradation behavior of jasmine flowers. These kinetic models were selected because they are widely applied in the analysis of color changes in biological materials during processing and storage [19,20,26,27,55,56]. These models' mathematical formulations capture different degradation patterns, from simple linear decay to more complex non-linear behaviors. By comparing multiple models, the study aimed to identify the most suitable model for accurately characterizing the dynamic color changes occurring during natural senescence. To assess the performance of each kinetic model in describing jasmine flower color degradation, their constants (C, C_0, k_0, k_1, and n), and goodness of fit were evaluated using three standard evaluation metrics, namely R^2, RMSE, and AIC. In this study, R^2 values obtained were >0.95, reflecting the strong explanatory power and quality of the fitted models. Conversely, the observed lower RMSE values indicated greater model precision and lower error margins. A lower AIC value (even negative values are encountered) signifies a more parsimonious and better performing model when comparing alternatives on the same dataset and avoids overfitting. Among these metrics, AIC is the most suitable indicator given its wider range of values and its mechanism of penalizing an increased number of independent variables and identifying the robust model. By concurrently employing all three metrics, we ensured a robust and multi-dimensional evaluation of the kinetic models. This comprehensive evaluation framework facilitates the reliable selection of the best model for each color index and flower component.

3.5.2. Developed Petal Models and Their Performance

The developed kinetic models for petals and derived constants with model performance parameters are presented in Table 4. Overall descriptive statistics across all color indices and model combinations, excluding models that did not perform adequately (e.g., the first-order model for ExG and ExGR color indices; $[12 \times 5] - 2 = 58$ models), were calculated. The range and mean $\pm$ standard deviation (STD) of these parameters were R^2: 0.80–0.99, 0.94 ± 0.05; RMSE: 0.36–1788.76, 96.06 ± 330.76; and AIC: -45.15–376.46, 53.75 ± 97.91. The STDs of RMSE and AIC were notably high, primarily due to outliers in the dataset (e.g., BI). Only for the BI, the RMSE and AIC were greater, which may be due to the fact that the range of BI values for the sample was 25,000–40,000, while the values of other indices were less than about 250. For BI, only the RMSE (572–1799) and AIC (323–376) with their higher values appeared to skew the performance, but the R^2 was in the range of 0.83–0.98. Furthermore, these performance measures, when normalized with the range of actual BI values, have similar performance to other indices. In this study, the indices were used directly, without normalization, a straightforward comparison was made, and BI was used because of its familiarity in color kinetics research.

Table 4. Color degradation kinetic models for jasmine flower petals and their performance developed using several color indices.

CI	Model	C_0	k_0	k_1	n	R^2	RMSE	AIC
ΔE	Zeroth-order	57.73	−2.39	-	-	0.98	2.41	48.03
	First-order	69.70	−0.09	-	-	0.97	3.01	59.15
	Exponential	-	−0.08	-	-	0.94	4.39	75.99
	Page	-	−0.03	-	1.44	0.98	2.36	46.88
	Peleg	63.85	−0.25	−0.01	-	0.99	1.30	19.19
CIVE	Zeroth-order	19.71	−0.57	-	-	0.95	0.93	0.14
	First-order	20.65	−0.04	-	-	0.89	1.40	20.90
	Exponential	-	−0.05	-	-	0.80	1.88	33.68
	Page	-	−0.01	-	2.14	0.94	1.05	6.40
	Peleg	18.22	−3.39	0.07	-	0.98	0.57	−21.78
VEG	Zeroth-order	35.56	−0.52	-	-	0.99	0.44	−37.46
	First-order	36.04	−0.02	-	-	0.98	0.58	−23.09
	Exponential	-	−0.06	-	-	0.87	1.39	18.38
	Page	-	−0.01	-	1.81	0.97	0.71	−13.26
	Peleg	34.96	−2.50	0.02	-	0.99	0.36	−45.15
ExG	Zeroth-order	15.83	−0.59	-	-	0.98	0.62	−20.28
	First-order	17.85	−0.07	-	-	-	-	-
	Exponential	-	−0.06	-	-	0.91	1.29	14.81
	Page	-	−0.01	-	1.55	0.97	0.74	−10.98
	Peleg	16.01	−1.59	−0.01	-	0.98	0.61	−18.62
ExGR	Zeroth-order	130.36	−1.85	-	-	0.96	2.63	52.42
	First-order	131.71	−0.02	-	-	-	-	-
	Exponential	-	−0.05	-	-	0.81	5.97	91.36
	Page	-	−0.01	-	2.18	0.95	2.92	57.51
	Peleg	125.70	−1.02	0.02	-	0.99	1.41	23.28
COM	Zeroth-order	34.38	−0.66	-	-	0.96	0.96	2.10
	First-order	35.04	−0.02	-	-	0.93	1.29	16.58
	Exponential	-	−0.05	-	-	0.81	2.12	39.52
	Page	-	−0.01	-	2.17	0.95	1.06	6.75
	Peleg	32.64	−3.00	0.06	-	0.99	0.47	−31.96
BI	Zeroth-order	41,239.93	−583.46	-	-	0.96	908.41	344.59
	First-order	41,659.85	−0.02	-	-	0.94	1092.28	353.80
	Exponential	-	−0.05	-	-	0.83	1788.76	376.46
	Page	-	−0.01	-	1.93	0.93	1106.97	354.47
	Peleg	39,794.62	−0.01	−0.01	-	0.98	572.43	323.49
WI	Zeroth-order	101.41	−1.60	-	-	0.95	2.50	49.88
	First-order	102.90	−0.02	-	-	0.94	2.90	57.21
	Exponential	-	−0.60	-	-	0.85	4.60	78.34
	Page	-	−0.01	-	1.72	0.93	3.09	60.44
	Peleg	98.67	−0.95	0.01	-	0.97	2.20	45.51
ISO_B	Zeroth-order	214.52	−2.46	-	-	0.99	2.15	42.25
	First-order	216.22	−0.01	-	-	0.98	2.62	52.13
	Exponential	-	−0.06	-	-	0.90	5.62	88.31
	Page	-	−0.01	-	1.51	0.95	3.82	70.97
	Peleg	211.55	−0.54	0.01	-	0.99	1.78	34.88
Hunter	Zeroth-order	46.84	−1.05	-	-	0.92	2.18	42.86
	First-order	48.34	−0.03	-	-	0.90	2.51	50.04
	Exponential	-	−0.06	-	-	0.85	3.09	58.46
	Page	-	−0.02	-	1.38	0.88	2.75	54.63
	Peleg	45.35	−1.34	0.02	-	0.93	2.07	42.34

Table 4. *Cont.*

CI	Model	C_0	k_0	k_1	n	R^2	RMSE	AIC
Hue	Zeroth-order	73.09	−1.12	-	-	0.97	1.45	22.64
	First-order	74.04	−0.02	-	-	0.95	1.83	34.21
	Exponential	-	−0.06	-	-	0.85	3.23	60.66
	Page	-	−0.01	-	1.86	0.95	1.92	36.65
	Peleg	70.82	−1.47	0.02	-	0.99	1.00	6.04
Chroma	Zeroth-order	18.29	−0.59	-	-	0.98	0.55	−25.68
	First-order	19.69	−0.05	-	-	0.93	1.13	10.27
	Exponential	-	−0.05	-	-	0.84	1.72	29.13
	Page	-	−0.00	-	2.04	0.97	0.69	−14.72
	Peleg	17.58	−2.23	0.02	-	0.99	0.46	−33.15

CI = Color index, C and C_0 are the initial and final color values of each color index, respectively. t = time in hour, and k_0, k_1, and n are the corresponding kinetic model constants. R^2 = coefficient of determination, RMSE = root mean squared error, and AIC = Akaike's information criteria. Zeroth-order model: $C = C_0 + k_0 t$; First-order model: $C = C_0 \exp(k_0 t)$; Exponential model: $C = \exp(-k_0 t)$; Page model: $C = \exp(-k_0 t^n)$; and Peleg model: $C = C_0 + \frac{t}{k_0 + k_1}$. Hunter = Hunter_WI color index.

Among the evaluated models, the Peleg and zeroth-order models consistently outperformed the others. Across all color indices, the Peleg model achieved the best performance (R^2: 0.93–0.99, 0.98 ± 0.02; RMSE: 0.36–572.43, 48.72 ± 164.93; and AIC: −45.15–323.49, 26.67 ± 98.07). In contrast, the exponential model generally underperformed, exhibiting lower R^2 values (0.80 in the CIVE index), indicating a poor fit and limited model efficiency. The Appendix A Figure A1 helps to readily visualize the results and compare the models' performance for petals based on significant selected performance metrics, such as R^2 and AIC. These findings underscore the robustness and generalizability of the Peleg model in modeling the color kinetics of jasmine petals, offering consistent and superior goodness of fit across nearly all color indices.

3.5.3. Developed Pedicle Models and Their Performance

The developed kinetic models for pedicles and determined constants with model performance parameters are presented in Table 5. Overall descriptive statistics across all color indices and model combinations, excluding the Peleg model with WI color index ($[12 \times 5] - 1 = 59$ models), were calculated. The evaluated range and mean ± STD of the overall descriptive statistics (across all color indices and model combinations, excluding the Peleg model with WI color index, $[12 \times 5] - 1 = 59$ models) were R^2: 0.79–0.99, 0.95 ± 0.05; RMSE: 0.28–688.36, 47.67 ± 169.63; and AIC: −59.51–330.72, 43.05 ± 87.37. As observed with petals, for pedicles, only for the BI, the RMSE (648–699) and AIC (327–330) were greater, but the R^2 was in the range of 0.93–0.94, indicating good performance.

The Peleg (except for BI) and Page models performed well across different color indices for pedicles compared to other models. Descriptive statistics evaluated among the color indices indicated strong predictive performance for Peleg (R^2: 0.96–0.99, 0.979 ± 0.008; and AIC: −49.54–65.25, 11.84 ± 37.36) and Page (R^2: 0.94–0.99, 0.969 ± 0.013; and AIC: −57.07–330.15, 41.29 ± 99.20) models. The Appendix A Figure A1 also presents the visualization of the various color index and kinetics model combinations for pedicles based on R^2 and AIC performance metrics. The better performances of the Peleg and Page models make them good candidates for modeling color kinetics in jasmine pedicles.

3.5.4. Overall Model Recommendations for Jasmine Flower Components

The modeling results revealed that the Peleg model was the most appropriate for describing color degradation kinetics in jasmine petals, while both Peleg and Page models exhibited strong performance for pedicles. The superiority of the Peleg model suggests that

the color degradation process is highly non-linear and time-dependent, which is consistent with previous findings on the complex biochemical and structural changes that occur during floral tissue drying. The Page model's superior performance for pedicle samples may be attributed to structural differences between petals and pedicles, where water loss and pigment degradation occur at varying rates. The relatively inadequate performance of the zeroth-order and first-order models across all indices indicates that simplistic decay assumptions were insufficient to capture the complexity of color changes in floral materials. These findings highlight the importance of selecting appropriate kinetic models based on tissue type and desired quality attributes. Understanding the kinetics of color degradation can guide optimization of fresh storage as well as drying protocols to preserve visual quality, thereby enhancing the commercial value of jasmine flowers in fresh and dried floral and cosmetic applications [25,57].

Table 5. Color degradation kinetic models for jasmine flower pedicles and their performance developed using several color indices.

CI	Model	C_0	k_0	k_1	n	R^2	RMSE	AIC
ΔE	Zeroth-order	19.68	−0.57	-	-	0.93	1.14	10.38
	First-order	21.71	−0.05	-	-	0.97	0.75	−10.10
	Exponential	-	−0.08	-	-	0.97	0.76	−11.67
	Page	-	−0.07	-	1.07	0.97	0.74	−11.34
	Peleg	23.01	−0.62	−0.04	-	0.97	0.68	−13.18
CIVE	Zeroth-order	13.90	−0.56	-	-	0.98	0.65	−17.37
	First-order	15.66	−0.08	-	-	0.88	1.40	20.81
	Exponential	-	−0.06	-	-	0.82	1.74	29.76
	Page	-	−0.01	-	2.26	0.97	0.66	−16.47
	Peleg	13.45	−2.13	0.01	-	0.98	0.62	−18.01
VEG	Zeroth-order	32.22	−0.41	-	-	0.96	0.62	−20.01
	First-order	32.68	−0.02	-	-	0.97	0.51	−29.41
	Exponential	-	−0.07	-	-	0.95	0.71	−14.85
	Page	-	−0.03	-	1.38	0.98	0.41	−41.02
	Peleg	33.71	−1.22	−0.04	-	0.98	0.39	−40.68
ExG	Zeroth-order	29.00	−1.29	-	-	0.96	2.01	38.89
	First-order	36.64	−0.10	-	-	0.95	2.15	42.21
	Exponential	-	−0.09	-	-	0.91	2.85	54.28
	Page	-	−0.02	-	1.65	0.98	1.24	14.76
	Peleg	33.29	−0.41	−0.01	-	0.98	1.36	21.24
ExGR	Zeroth-order	103.48	−2.11	-	-	0.95	3.40	65.14
	First-order	105.62	−0.03	-	-	1.00	4.56	-
	Exponential	-	−0.05	-	-	0.79	7.19	100.67
	Page	-	−0.01	-	2.49	0.97	2.86	56.62
	Peleg	98.11	−0.91	0.02	-	0.99	1.90	38.01
COM	Zeroth-order	24.78	−0.78	-	-	0.95	1.22	14.06
	First-order	26.10	−0.05	-	-	0.88	2.01	38.98
	Exponential	-	−0.05	-	-	0.79	2.64	50.47
	Page	-	−0.01	-	2.47	0.97	1.03	5.58
	Peleg	22.86	−2.41	0.05	-	0.98	0.70	−11.49
BI	Zeroth-order	31127.09	−348.12	-	-	0.93	688.36	330.72
	First-order	31431.41	−0.01	-	-	0.94	655.00	328.23
	Exponential	-	−0.07	-	-	0.93	669.80	327.35
	Page	-	−0.09	-	0.91	0.94	648.18	327.71
	Peleg	-	-	-	-	-	-	-

Table 5. *Cont.*

CI	Model	C_0	k_0	k_1	n	R^2	RMSE	AIC
WI	Zeroth-order	95.34	−1.31	-	-	0.95	2.05	39.96
	First-order	96.87	−0.02	-	-	0.97	1.76	32.31
	Exponential	-	−0.07	-	-	0.97	1.80	31.31
	Page	-	−0.05	-	1.11	0.97	1.65	29.18
	Peleg	100.05	−0.38	−0.01	-	0.98	1.48	25.72
ISO_B	Zeroth-order	188.94	−2.00	-	-	0.97	2.60	51.82
	First-order	190.56	−0.01	-	-	0.97	2.34	46.55
	Exponential	-	−0.07	-	-	0.96	2.89	55.14
	Page	-	−0.05	-	1.11	0.97	2.70	53.58
	Peleg	193.74	−0.31	−0.01	-	0.98	2.12	43.54
Hunter	Zeroth-order	58.69	−1.53	-	-	0.82	5.22	86.64
	First-order	64.81	−0.04	-	-	0.90	3.93	72.38
	Exponential	-	−0.13	-	-	0.97	2.01	36.88
	Page	-	−0.13	-	1.00	0.97	2.01	38.86
	Peleg	28.50	−0.08	−0.01	-	0.98	1.84	36.51
Hue	Zeroth-order	17.33	−0.39	-	-	0.98	0.43	−38.14
	First-order	18.14	−0.03	-	-	0.99	0.30	−56.02
	Exponential	-	−0.07	-	-	0.89	0.96	−0.10
	Page	-	−0.01	-	1.83	0.99	0.28	−59.51
	Peleg	18.17	−1.66	−0.03	-	0.99	0.31	−53.19
Chroma	Zeroth-order	93.48	−2.20	-	-	0.96	3.24	62.71
	First-order	97.07	−0.03	-	-	0.94	4.07	74.18
	Exponential	-	−0.05	-	-	0.83	6.60	96.34
	Page	-	−0.01	-	1.89	0.95	3.62	68.30
	Peleg	90.71	−0.61	0.01	-	0.96	3.04	61.59

CI = Color index, C and C_0 are the initial and final color values of each color index, respectively. t = time in hour, and k_0, k_1, and n are the corresponding kinetic model constants. R^2 = coefficient of determination, RMSE = root mean squared error, and AIC = Akaike's information criteria. Zeroth-order model: $C = C_0 + k_0 t$; First-order model: $C = C_0 \exp(k_0 t)$; Exponential model: $C = \exp(-k_0 t)$; Page model: $C = \exp(-k_0 t^n)$; and Peleg model: $C = C_0 + \frac{t}{k_0 + k_1}$. Hunter = Hunter_WI color index.

3.6. Color Degradation Kinetics Data and Model Visualization

The color degradation plots of jasmine petals and pedicles with their kinetic models are shown in Figures 7 and 8. It can be noted in both the cases of petals and pedicle graphs that all the color indices (ΔE, CIVE, VEG, ExG, ExGR, COM, BI, WI, ISO_B, Hunter_WI, hue, and Ch) are showing a declining trend, indicating color loss in jasmine flowers with time. The decrease in total color difference value (ΔE) represents the cumulative changes in the overall color value of the flowers (petals and pedicles), likely due to the aging or environmental factors. A slight concave trend in a few color indices (CIVE, ExG, and VEG) implies rapid initial changes in the color values that stabilize over time, possibly linked to chlorophyll pigments activity and concentration. In ExGR and COM indices, a continuous shift in their green intensities might be the reason for the linearly declining trend in the data points. There is a steep change in the browning index values that reflect the ongoing reactions due to oxidation or pigment degradation, and non-pigmented parenchyma cells tissue is oxidized with time. Due to the changes in the surface reflectance, a falling trend in WI, ISO_B, and Hunter_WI was recorded. Similar changes in hue and chroma indices were seen, indicating progressive shifts in their color intensities. The observed patterns, whether concave, convex, or linear, provide insight into underlying physiological or chemical changes such as pigment oxidation, chlorophyll degradation, or surface reflectance dynamics, offering valuable perspectives on temporal changes in the color indices.

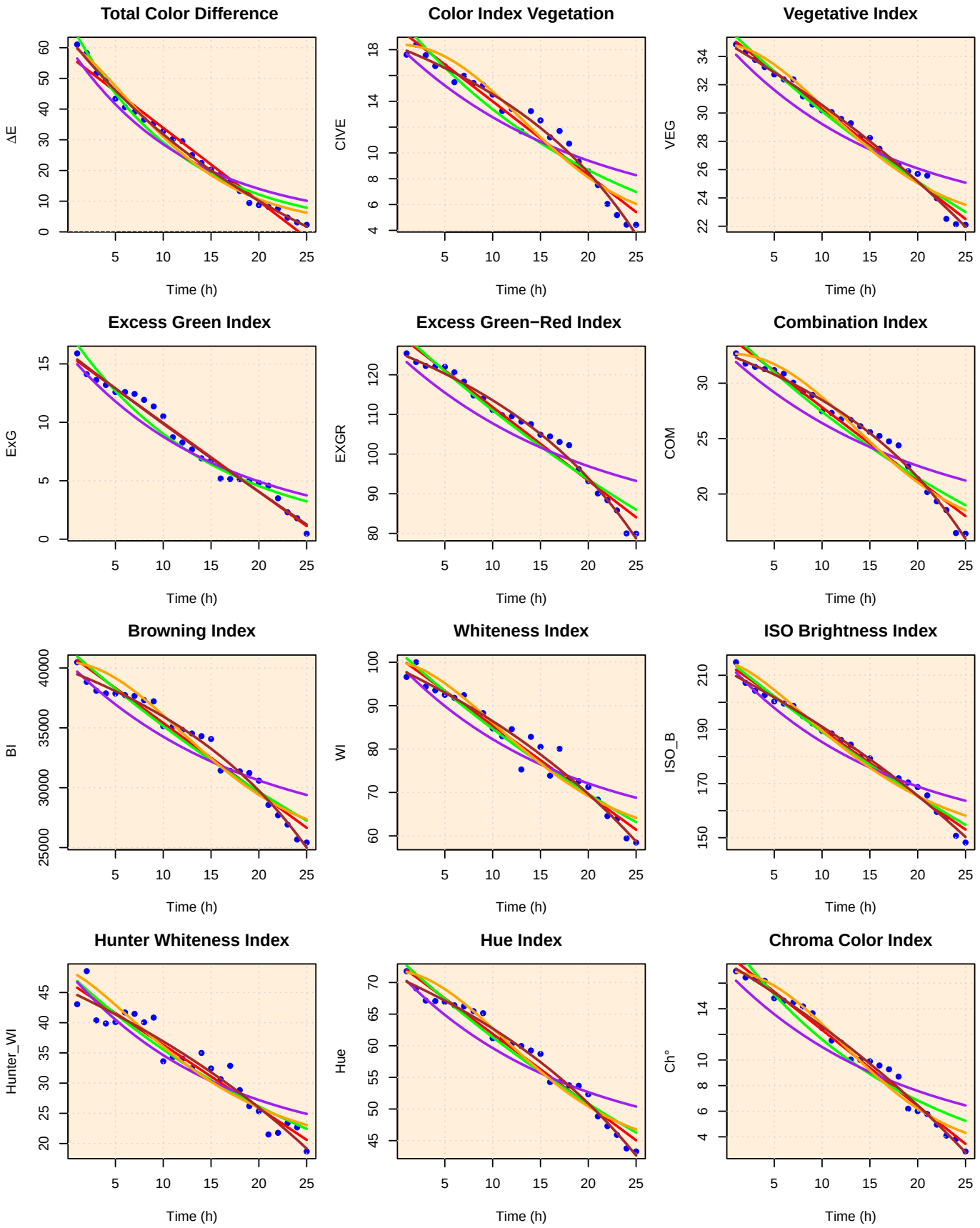


Figure 7. Color degradation kinetics plots of jasmine petals for different color indices. Legend: ● Data; — Zeroth-order model; — First-order model; — Exponential model; — Page model; — Peleg model.

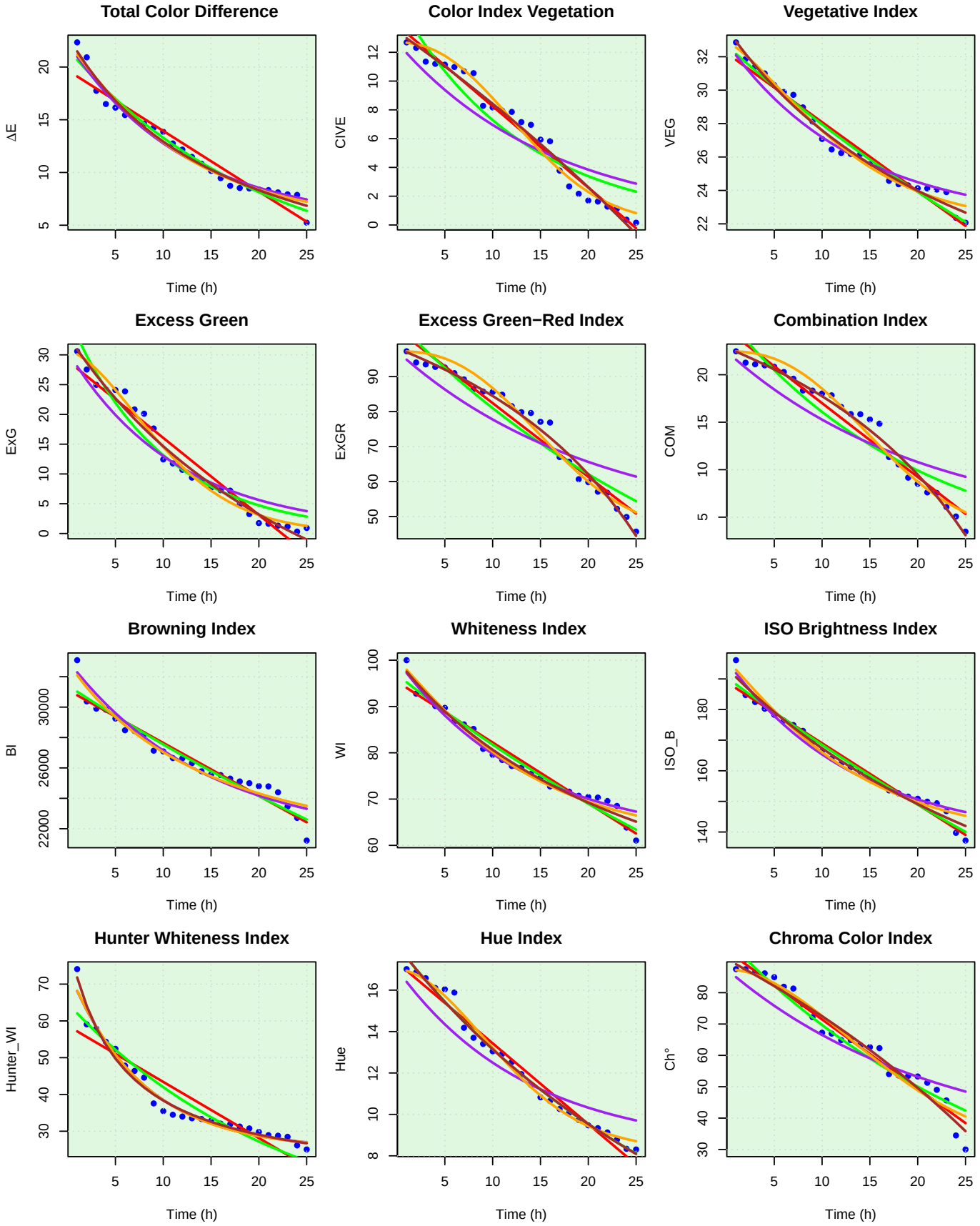


Figure 8. Color degradation kinetics plots of jasmine pedicles for different color indices. Legend: ● Data; — Zeroth-order model; — First-order model; — Exponential model; — Page model; — Peleg model.

The modeling of color degradation kinetics revealed that the Peleg kinetic model provided the best fit for most of the color indices, effectively capturing the dynamics of degradation. Additionally, the exponential and Page models exhibited strong performance for certain indices, demonstrating their utility in describing complex degradation behaviors. For jasmine petals, the Peleg model showed superior predictive capability for indices such as ΔE, CIVE, VEG, ExGR, COM, BI, WI, ISO_B, hue, and chroma, respectively. This result underscores the robustness of the model in capturing the gradual degradation of floral pigments in jasmine petals during their natural senescence.

For pedicles, models such as exponential, Page, Peleg, and zeroth performed well for various color indices. The Page model provided an excellent fit for indices, such as VEG, ExG, and Hue, while the Peleg model remained consistent across most parameters, like ExGR, COM, WI, and ISO_B, respectively. The relatively accelerated rates of degradation observed in pedicles align with their structural vulnerability to environmental stressors and moisture loss.

3.7. Color Degradation Kinetics Model Performance Comparison and Ranking

One way of comparing the performance of the models (60 models) is to rank them based on the performance metrics utilized (R^2, RMSE, and AIC). The model ranks are arranged for each flower component, featuring all the 12 color indices along with their performance metrics as presented in Table 6.

Table 6. Ranked kinetic models to estimate color degradation of jasmine flowers components.

Component	Rank	CI	Model	Best Fitted Model	R^2	RMSE	AIC
Petals	1	VEG	Peleg	$C = 34.96 + \frac{t}{-2.50+0.02}$	0.99	0.35	−45.15
	2	Chroma	Peleg	$C = 17.58 + \frac{t}{-2.23+0.02}$	0.98	0.45	−33.15
	3	COM	Peleg	$C = 32.64 + \frac{t}{-3+0.06}$	0.99	0.46	−31.96
	4	CIVE	Peleg	$C = 18.22 + \frac{t}{-3.39+0.07}$	0.98	0.57	−21.78
	5	ExG	Zeroth	$C = 15.83 - 0.59 \cdot t$	0.97	0.61	−20.28
	6	Hue	Peleg	$C = 70.82 + \frac{t}{-1.47+0.02}$	0.98	1.00	6.04
	7	Delta E	Peleg	$C = 63.85 + \frac{t}{-0.25-0.01}$	0.99	1.30	19.19
	8	ExGR	Peleg	$C = 125.70 + \frac{t}{-1.02+0.02}$	0.98	1.41	23.28
	9	ISO_B	Peleg	$C = 211.55 + \frac{t}{-0.54+0.01}$	0.99	1.78	34.88
	10	Hunter_WI	Zeroth	$C = 46.84 - 1.05 \cdot t$	0.92	2.17	42.86
	11	WI	Peleg	$C = 98.67 + \frac{t}{-0.95+0.01}$	0.96	2.20	45.51
	12	BI *	Peleg	$C = 39794.62 + \frac{t}{-0.001-0.001}$	0.98	572.42	323.49
Pedicles	1	Hue	Page	$C = e^{-0.07 \cdot t^{1.83}}$	0.99	0.28	−59.51
	2	VEG	Page	$C = e^{-0.03 \cdot t^{1.38}}$	0.98	0.40	−41.02
	3	CIVE	Zeroth	$C = 13.90 - 0.56 \cdot t$	0.97	0.65	−17.36
	4	Delta E	Exponential	$C = e^{-0.08 \cdot t}$	0.96	0.76	−11.67
	5	COM	Peleg	$C = 22.86 + \frac{t}{-2.41+0.05}$	0.98	0.70	−11.48
	6	ExG	Page	$C = e^{-0.02 \cdot t^{1.65}}$	0.98	1.24	14.76
	7	WI	Peleg	$C = 100.05 + \frac{t}{-0.38+0.01}$	0.97	1.48	25.72
	8	Hunter_WI	Exponential	$C = e^{-0.13 \cdot t}$	0.97	2.00	36.88
	9	ExGR	Peleg	$C = 98.11 + \frac{t}{-0.91+0.02}$	0.98	1.89	38.01
	10	ISO_B	Peleg	$C = 193.74 + \frac{t}{-0.31-0.01}$	0.97	2.11	43.54
	11	Chroma	Zeroth	$C = 93.48 - 2.20 \cdot t$	0.96	3.23	62.71
	12	BI *	Exponential	$C = e^{-0.07 \cdot t}$	0.93	669.79	327.35

CI = Color index (Table 2), C = predicted color value of different kinetic models (Table 2), t = independent variable time in h, R^2 = coefficient of determination, RMSE = root mean squared error, and AIC = Akaike's information criteria. * BI (browning index) was ranked low based on high RMSE and AIC scores, and one of the possible reasons, among others, is its high range of values (25,000–40,000) compared to other color indices (Section 3.5.2).

3.7.1. Jasmine Petals

Among the models tested, for petals, the Peleg model ranked the highest and consistently provided the best fit for most color indices (10 out of 12), achieving an R^2 of 0.99 for VEG, COM, ΔE, and ISO_B. However, the best four color indices with the Peleg model for petals were VEG, chroma, COM, and CIVE, having RMSE $\leq$ 0.57, and AIC $\leq$ 21.78 (Table 6). Zeroth-order is another model that was found suitable for petals with color indices ExG ($R^2 = 0.97$, AIC $= -20.28$) and Hunter_WI ($R^2 = 0.92$, AIC $= 40.86$). While indices like ΔE, ExGR, and ISO_B also exhibited high R^2 values (>0.98), they were associated with relatively higher RMSE and AIC values, suggesting these indices were less effective for precise predictions.

As outlined earlier, the BI index based on the BI value range and considerations made in the study, although having a high R^2 of 0.98, was ranked the lowest due to its extremely high RMSE (572.42) and positive AIC (323.49) for this straightforward analysis. It is possible to improve the BI model ranking when the values are normalized, which is not followed in this study. These results highlight that the VEG index, paired with the Peleg model, offered the best predictive capability for color degradation in jasmine petals, and other promising indices included chroma, COM, and CIVE.

3.7.2. Jasmine Pedicles

For jasmine pedicles, the Page model combined with the hue color index emerged as the best performer ($R^2 = 0.99$, RMSE = 0.28, AIC $= -59.51$). The other models that were suitable for pedicle color degradation are zeroth-order, exponential, and Peleg. The VEG color index, also fitted with the Page model, showed similarly strong predictive capability ($R^2 = 0.98$, RMSE = 0.40, AIC $= -41.02$). The zeroth-order model with CIVE, exponential with ΔE, and Peleg with COM also demonstrated satisfactory performance for the pedicles (R^2: 0.96–98, RMSE: 0.65–0.76, AIC: -17.36–-11.48). As observed with petals, the BI model again was ranked last ($R^2 = 0.93$, RMSE = 669.79, AIC $= 327.35$). It can be concluded that hue and VEG color indices paired with the Page model exhibited the highest performance, indicating superior model fitting and lower prediction errors, hence recommended for kinetics applications.

These findings align with previous studies, such as kinetic models for color kinetics of milled industrial beet [27], identification and profiling of microalgae species [26], and color kinetics of infrared drying or rose flower petals [25]. The statistical analysis thus confirms the robustness and applicability of the selected kinetic models, underscoring their potential for predicting color degradation and informing strategies to enhance the postharvest quality and longevity of jasmine flowers.

The suggested models for petals and pedicles depict degradation patterns under standardized conditions and do not incorporate variations due to environmental or biochemical drivers known to accelerate floral senescence [58]. Therefore, the results provide a context-specific description of jasmine flower color change under passive indoor conditions, which are representative of common storage conditions. Although the model enables comparison between petal and pedicle kinetics, it is not designed for predictive generalization across varying postharvest environments; however, the methodologies outlined (e.g., sample layout, image acquisition, preprocessing, computer vision analysis, color degradation kinetics, and output generation; Figure 2) can be readily employed to other conceivable environmental condition variations and realistic prediction model development.

4. Suggestions for Future Research

To further enhance the research and practical applications of the findings, a novel Java-based plugin needs to be developed that can separate the jasmine petals and pedicles

automatically before the color analysis, overcoming the manual segmentation process. Future studies should broaden the methodology to encompass other ornamental flower species to generalize the results. Incorporating additional environmental variables, such as humidity and temperature, will provide a more comprehensive understanding of color degradation. Exploring preservation treatments, including controlled atmosphere storage and chemical treatments, can help extend the shelf life of jasmine flowers. Future work should include multi-sensor data (e.g., temperature-loggers, gas composition sensors) to build comprehensive predictive models and perform their validation. Integrating advanced image processing techniques, such as deep learning algorithms, will improve the accuracy of detecting subtle color variations. Developing real-time monitoring systems utilizing IoT-enabled image sensors will facilitate continuous tracking of flower degradation, enabling optimized storage conditions. Additionally, correlating computer vision analysis with biochemical studies will offer insights into the metabolic pathways involved in pigment degradation. Enhancing supply chain management practices based on these findings will improve handling, packaging, and transportation within the floral industry. Expanding the dataset with diverse flower varieties under varying environmental conditions will strengthen the predictive capabilities of the models, contributing to more efficient postharvest management and commercial viability of perishable floral commodities.

5. Conclusions

This study presents a novel, cost-effective, and automated approach for analyzing the color degradation kinetics of jasmine flower components (petals and pedicles) using a user-coded computer vision image analysis tool integrated with the ImageJ platform. From the experiments, with images taken at 1 h intervals up to 25 h, it was observed that the flowers started to bloom from the 3rd hour, and a notable color change in the flowers was observed from the 12th hour. The developed plugin adeptly distinguished the petals from the pedicles based on the area (petals $\geq 19\,mm^2 >$ pedicles), thereby enabling analysis of each component. The RGB values recorded, based on the mean pixel colors, for petals and pedicles separately were used to derive twelve color indices (ΔE, CIVE, VEG, ExG, ExGR, COM, BI, WI, ISO_B, Hunter_WI, hue, and chroma), which were subsequently fitted with kinetic models (zeroth-order, first-order, exponential, Page, and Peleg models with constants C, C_0, k_0, k_1, and n) to evaluate the color degradation behavior over time, and model performance metrics (R^2, RMSE, and AIC) were successfully evaluated.

The systematic ranking of models and indices allowed the identification of optimal models for different flower components, balancing complexity with predictive accuracy. Significant outcomes of this investigation reveal that the VEG color index is exceptionally effective in quantifying the color degradation of jasmine petals ($R^2 = 0.99$, RMSE = 0.35). The Peleg model exhibited the most favorable fit for the majority of color indices in jasmine petals, accurately depicting the temporal color alterations. For jasmine pedicles, the hue color index ranked first (low AIC $= -59.51$). A differential color degradation kinetic pattern was observed between petals and pedicles. Jasmine petals exhibited higher pigment stability, retaining their color integrity for a longer duration, whereas pedicles exhibited a more rapid decline in color indices within 25 h study period.

The developed computer vision plugin effectively characterized the temporal progression of floral senescence, paving the way for broader applications in postharvest physiology and floriculture research. Future research should focus on developing fully automated segmentation algorithms capable of distinguishing petals and pedicles without manual intervention. Expanding the dataset to other jasmine varieties and varying environmental conditions will enhance the robustness of the kinetic models. These advancements and future integration of the computer vision methodology will contribute to more precise

postharvest management strategies, operational scalability, and the extension of the shelf life and visual appeal of jasmine and other perishable floral commodities.

Author Contributions: Conceptualization, H.T., and C.I.; methodology, H.T., T.T., A.J., Z.Z. and C.I.; formal analysis, H.T.; investigation, H.T.; resources, C.I., J.R.H. and D.W.A.; data curation, H.T.; writing—original draft preparation, H.T., T.T., A.J. and C.I.; writing—review and editing, H.T., T.T., A.J., C.I., A.A.-B., Z.Z., C.W.W., D.A.S., J.R.H., D.W.A., L.O.P. and S.S.; visualization, H.T., T.T., A.J. and C.I.; supervision, C.I.; project administration, C.I.; funding acquisition, C.I., J.R.H. and D.W.A. All authors have read and agreed to the published version of the manuscript.

Funding: This research was a contribution from the Long-Term Agroecosystem Research (LTAR) network, LTAR is supported by the United States Department of Agriculture, Fund No: FAR0036174. The work was also supported by USDA NIFA Hatch Project: ND01493. NGPRL research is funded by ARS project number 3064-21600-001-000D.

Data Availability Statement: The dataset used for the analysis of the study is available in Mendeley Data (DOI: https://doi.org/10.17632/42p3sxt73r.1). It contains time-series RGB values of color images of jasmine flowers over 25 h of natural storage. The RGB values were derived by employing user-coded ImageJ plugin program. Sheet 1 of the file contains the jasmine flower petals RGB values of 4 samples collected for 25 h, while Sheet 2 contains the jasmine flower pedicles RGB values (4 samples, 25 h). Sheet 3 contains the consolidated data of RGB values and the derived 12 color indices used for the color degradation kinetics modeling (5 models) of jasmine flower components.

Acknowledgments: The administrative support extended by NGPRL staff and the lab facilities utilized in this effort are gratefully acknowledged. This research was a contribution from the Long-Term Agroecosystem Research (LTAR) network. LTAR is supported by the United States Department of Agriculture.

Conflicts of Interest: The authors declare no conflicts of interest. NDSU and USDA are equal opportunity providers and employers. The mention of trade names of commercial products in this article is solely for the purpose of providing factual information and does not imply recommendation or endorsement by the NDSU or the USDA.

Appendix A. Visualization of Kinetic Model Performance of Jasmine Petals and Pedicles Using Selected Metrics

To facilitate a more intuitive comparison of kinetic model performance across various color indices, heatmap visualizations of the selected evaluation metrics (R^2 and AIC; Tables 4 and 5) for both petals and pedicles are presented in Figure 8. In the heatmap visualization, darker shades indicate higher R^2 and lower AIC values, both representing better performance metrics. From the heatmaps, it is evident that the Peleg model consistently achieved the highest R^2 and lowest AIC values (darker shades) across most color indices, especially for petals. The Page model also performed strongly for pedicles. In contrast, the exponential and first-order models exhibited relatively poorer fit (lighter shades) for several indices.

These summaries facilitate visual comparison of the entire results (Tables 4 and 5) and not only readily identify the best performing model but also reveal model performance trends across multiple indices and flower components.

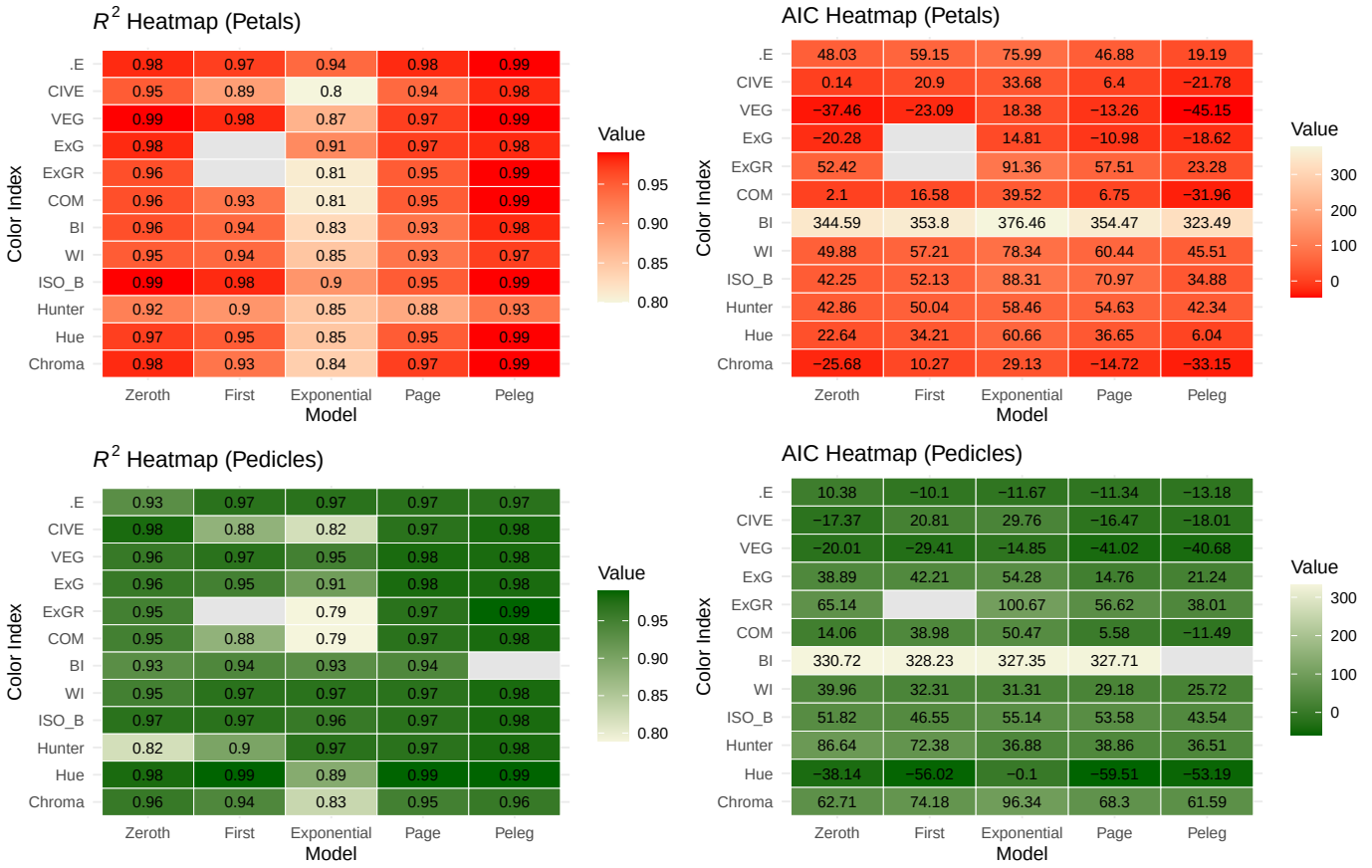


Figure A1. Heatmap visualization of jasmine petals and pedicles of R^2 and AIC (Akaike's information criteria) for different color indices and model performance combinations. The gaps indicate the models' non-convergence, resulting in the absence of performance metrics.

References

1. Barad, A.; Gandamalla, M.; Maheta, P. Role of rural women in post-harvest handling and export of jasmine flower. *Univers. J. Agric. Res.* **2017**, *5*, 329–332.
2. Zhang, Y.J.; Liu, Y.Q.; Pu, X.Y.; Yang, C.R. Iridoidal glycosides from *Jasminum sambac*. *Phytochemistry* **1995**, *38*, 899–903.
3. Qur'ania, A.; Sarinah, I. Identification of jasmine flower (*Jasminum* sp.) based on the shape of the flower using sobel edge and k-nearest neighbour. *IOP Conf. Ser. Mater. Sci. Eng.* **2018**, *332*, 012008. [CrossRef]
4. Heikal, G.; Abd-Elatef, E.A. Effect color of jasmine flowers on the infestation by macrosiphum rosae and tetranychus urticae under glasshouse conditions. *Egypt. Acad. J. Biol. Sci. A Entomol.* **2021**, *14*, 219–226. [CrossRef]
5. Ray, H.; Majumdar, S.; Biswas, S.P.; Das, A.; Ghosh, T.; Ghosh, A. Characterization of the volatile aroma compounds from the concrete and jasmine flowers grown in India. *Chem. Eng. Trans.* **2014**, *40*, 265–270.
6. Jawaharlal, M.; Thamaraiselvi, S.; Ganga, M. Packaging technology for export of jasmine (*Jasminum sambac* Ait.) Flowers. *J. Hortic. Sci.* **2012**, *7*, 180–189. [CrossRef]
7. Ali, S.M.; Nidoni, U.; Palanimuthu, S.H.; Ramappa, K.; Ramesh, G.; Naik, N. Enhancing shelf life and freshness retention in jasmine flowers (*Jasminum multiflorum* L.) Through Post-Harvest Chem. Treat. *Int. J. Adv. Biochem. Res.* **2024**, *8* (Suppl. 3), 265–270. [CrossRef]
8. Ray, H.; Majumdar, S.; Das, A.; Bhattacharyya, N.; Kumar, S.; Bhattacharjya, R. Aroma quality evaluation of jasmine flower. In Proceedings of the 2014 International Conference on Control, Instrumentation, Energy and Communication (CIEC), Calcutta, India, 31 January–2 February 2014; pp. 598–602.
9. Issa, M.Y.; Mohsen, E.; Younis, I.Y.; Nofal, E.S.; Farag, M.A. Volatiles distribution in jasmine flowers taxa grown in Egypt and its commercial products as analyzed via solid-phase microextraction (SPME) coupled to chemometrics. *Ind. Crop. Prod.* **2020**, *144*, 112002. [CrossRef]
10. Mohanasundari, P.; Sivakumar, T.; Krishna Surendar, K. Effect of post-harvest treatment and storage temperature on fragrance of jasmine (*J. grandiflorum*). *Ann. Plant Sci.* **2018**, *7*, 2391–2393.

11. Yathindra, H.; Keerthishankar, K.; Rajesh, A.; Harshavardhan, M.; Mutthuraju, G.; Mangala, K. Packaging technology for extending shelf life of jasmine (*Jasminum sambac* CV. Mysuru Mallige) Flowers. *J. Pharmacogn. Phytochem.* **2018**, *7*, 257–259.
12. Cubero, S.; Aleixos, N.; Moltó, E.; Gómez-Sanchis, J.; Blasco, J. Advances in machine vision applications for automatic inspection and quality evaluation of fruits and vegetables. *Food Bioprocess Technol.* **2011**, *4*, 487–504. [CrossRef]
13. El-Mesery, H.S.; Mao, H.; Abomohra, A.E.F. Applications of non-destructive technologies for agricultural and food products quality inspection. *Sensors* **2019**, *19*, 846. [CrossRef] [PubMed]
14. Shajahan, S. Agricultural Field Applications of Digital Image Processing Using an Open Source ImageJ Platform. Ph.D. Thesis, North Dakota State University, Fargo, ND, USA, 2019.
15. Chen, F.; Li, Y.; Sun, H.; Wei, Q.; Fang, C.; Lin, X.; Li, Y.; Chen, Z.; Lin, H.; Cao, Z. Petal damage and bent flower detection method of rose cut flowers based on computer vision. *Sci. Hortic.* **2025**, *340*, 113927. [CrossRef]
16. Brosnan, T.; Sun, D.W. Improving quality inspection of food products by computer vision—A review. *J. Food Eng.* **2004**, *61*, 3–16. [CrossRef]
17. Mery, D.; Arteta, C. Automatic defect recognition in X-ray testing using computer vision. In Proceedings of the 2017 IEEE Winter Conference on Applications of Computer Vision (WACV), Santa Rosa, CA, USA, 24–31 March 2017; pp. 1026–1035.
18. Sharayei, P.; Hedayatizadeh, M.; Chaji, H.; Einafshar, S. Studying the thin-layer drying kinetics and qualitative characteristics of dehydrated saffron petals. *J. Food Process. Preserv.* **2018**, *42*, e13677. [CrossRef]
19. Jiang, T.; Mao, Y.; Sui, L.; Yang, N.; Li, S.; Zhu, Z.; Wang, C.; Yin, S.; He, J.; He, Y. Degradation of anthocyanins and polymeric color formation during heat treatment of purple sweet potato extract at different pH. *Food Chem.* **2019**, *274*, 460–470.
20. Rasane, P.; Singh, A.; Singh, J.; Kaur, S.; Nanda, V.; Kaur, J.; Gunjal, M.; Bhadariya, V.; Ercisli, S.; Ullah, R.; et al. Image analysis-based discoloration rate quantification and kinetic modeling for shelf-life prediction in herb-coated pear slices. *Sci. Rep.* **2024**, *14*, 1647.
21. Palumbo, M.; Pace, B.; Cefola, M.; Montesano, F.F.; Colelli, G.; Attolico, G. Non-destructive and contactless estimation of chlorophyll and ammonia contents in packaged fresh-cut rocket leaves by a Computer Vision System. *Postharvest Biol. Technol.* **2022**, *189*, 111910. [CrossRef]
22. Schroeder, A.B.; Dobson, E.T.; Rueden, C.T.; Tomancak, P.; Jug, F.; Eliceiri, K.W. The ImageJ ecosystem: Open-source software for image visualization, processing, and analysis. *Protein Sci.* **2021**, *30*, 234–249. [CrossRef]
23. Ratti, C. Hot air and freeze-drying of high-value foods: A review. *J. Food Eng.* **2001**, *49*, 311–319. [CrossRef]
24. Vega-Gálvez, A.; Di Scala, K.; Rodríguez, K.; Lemus-Mondaca, R.; Miranda, M.; López, J.; Perez-Won, M. Effect of air-drying temperature on physico-chemical properties, antioxidant capacity, colour and total phenolic content of red pepper (*Capsicum annuum*, L. var. Hungarian). *Food Chem.* **2009**, *117*, 647–653. [CrossRef]
25. Aradwad, P.; Yadav, R.; Arun Kumar, T.; Shabeer, T.A.; Raju, D.; Kumar, P.N.; Sahoo, M. Mass transfer and color change kinetics of infrared drying of rose petals and its impact on physico-chemical properties. *J. Food Process Eng.* **2023**, *46*, e14359. [CrossRef]
26. Sunoj, S.; Hammed, A.; Igathinathane, C.; Eshkabilov, S.; Simsek, H. Identification, quantification, and growth profiling of eight different microalgae species using image analysis. *Algal Res.* **2021**, *60*, 102487.
27. Pothula, A.K.; Igathinathane, C.; Shen, J.; Nichols, K.; Archer, D. Milled industrial beet color kinetics and total soluble solid contents by image analysis. *Ind. Crop. Prod.* **2015**, *65*, 159–169. [CrossRef]
28. Suh, H.J.; Noh, D.O.; Kang, C.S.; Kim, J.M.; Lee, S.W. Thermal kinetics of color degradation of mulberry fruit extract. *Food/Nahrung* **2003**, *47*, 132–135. [CrossRef] [PubMed]
29. Peleg, M.; Normand, M.D.; Dixon, W.R.; Goulette, T.R. Modeling the degradation kinetics of ascorbic acid. *Crit. Rev. Food Sci. Nutr.* **2018**, *58*, 1478–1494.
30. Peleg, M.; Normand, M.D.; Corradini, M.G. A new look at kinetics in relation to food storage. *Annu. Rev. Food Sci. Technol.* **2017**, *8*, 135–153. [CrossRef]
31. Loypimai, P.; Moongngarm, A.; Chottanom, P. Thermal and pH degradation kinetics of anthocyanins in natural food colorant prepared from black rice bran. *J. Food Sci. Technol.* **2016**, *53*, 461–470. [CrossRef]
32. Peleg, M. An empirical model for the description of moisture sorption curves. *J. Food Sci.* **1988**, *53*, 1216–1217. [CrossRef]
33. Madamba, P.S.; Driscoll, R.H.; Buckle, K.A. The thin-layer drying characteristics of garlic slices. *J. Food Eng.* **1996**, *29*, 75–97.
34. Durand, L.B.; Ruiz-López, J.; Perez, B.G.; Ionescu, A.M.; Carrillo-Pérez, F.; Ghinea, R.; Pérez, M.M. Color, lightness, chroma, hue, and translucency adjustment potential of resin composites using CIEDE2000 color difference formula. *J. Esthet. Restor. Dent.* **2021**, *33*, 836–843. [CrossRef] [PubMed]
35. Ahn, J.S.; Lee, Y.K. Color distribution of a shade guide in the value, chroma, and hue scale. *J. Prosthet. Dent.* **2008**, *100*, 18–28. [CrossRef]
36. Pathare, P.B.; Opara, U.L.; Al-Said, F.A.J. Colour measurement and analysis in fresh and processed foods: A review. *Food Bioprocess Technol.* **2013**, *6*, 36–60.
37. Gao, S.; Yan, K.; Liu, J.; Pu, J.; Zou, D.; Qi, J.; Mu, X.; Yan, G. Assessment of remote-sensed vegetation indices for estimating forest chlorophyll concentration. *Ecol. Indic.* **2024**, *162*, 112001. [CrossRef]

38. Barani, Y.H.; Zhang, M.; Wang, B. Effect of thermal and ultrasonic pretreatment on enzyme inactivation, color, phenolics and flavonoids contents of infrared freeze-dried rose flower. *J. Food Meas. Charact.* **2021**, *15*, 995–1004. [CrossRef]
39. He, Y.; Guo, X.; Lu, R.; Niu, B.; Pasapula, V.; Hou, P.; Cai, F.; Xu, Y.; Chen, F. Changes in morphology and biochemical indices in browning callus derived from *Jatropha Curcas* Hypocotyls. *Plant Cell Tissue Organ Cult. (PCTOC)* **2009**, *98*, 11–17. [CrossRef]
40. Nash, J.C.; Bhattacharjee, A. A comparison of R tools for nonlinear least squares modeling. *R J.* **2023**, *15*, 198–215.
41. Kuha, J. AIC and BIC: Comparisons of assumptions and performance. *Sociol. Methods Res.* **2004**, *33*, 188–229. [CrossRef]
42. Vrieze, S.I. Model selection and psychological theory: A discussion of the differences between the Akaike information criterion (AIC) and the Bayesian information criterion (BIC). *Psychol. Methods* **2012**, *17*, 228. [CrossRef]
43. Wickham, H. *Advanced R*; Chapman and Hall/CRC: London, UK, 2019.
44. Farhood, H.; Bakhshayeshi, I.; Pooshideh, M.; Rezvani, N.; Beheshti, A. Recent advances of image processing techniques in agriculture. In *Artificial Intelligence and Data Science in Environmental Sensing*; Elsevier: Amsterdam, The Netherlands, 2022; pp. 129–153.
45. Bhambri, P.; Singh, S.; Jain, S.; Dhanoa, I.S. Plants recognition using leaf image pattern analysis with focus on advanced smart computing technologies. *AIP Conf. Proc.* **2023**, *2916*, 020003.
46. Bej, G.; Pal, A.; Dey, T.; Majumdar, S.; Akuli, A.; Ghosh, A.; Bhattacharyya, N. Extraction of appearance-based DUS characteristics of okra stem, flower, and seed using image processing. In Proceedings of the International Conference on Computational Intelligence, Data Science and Cloud Computing: IEM-ICDC 2021, Kolkata, India, 22–24 December 2021; Springer: Singapore, 2022; pp. 209–223.
47. Pintó-Marijuan, M.; Munné-Bosch, S. Photo-oxidative stress markers as a measure of abiotic stress-induced leaf senescence: Advantages and limitations. *J. Exp. Bot.* **2014**, *65*, 3845–3857. [CrossRef] [PubMed]
48. Manzoor, A.; Bashir, M.A.; Naveed, M.S.; Akhtar, M.T.; Saeed, S. Postharvest chemical treatment of physiologically induced stem end blockage improves vase life and water relation of cut flowers. *Horticulturae* **2024**, *10*, 271. [CrossRef]
49. Sukpitak, C.; Seraypheap, K.; Muñoz, P.; Munné-Bosch, S. Influence of water deficit on the longevity of ethylene-sensitive and ethylene-insensitive flowers. *Environ. Exp. Bot.* **2024**, *219*, 105647. [CrossRef]
50. Da Silva, J.T. The cut flower: Postharvest considerations. *J. Biol. Sci.* **2003**, *3*, 406–442.
51. Salunkhe, D.K.; Bhat, N.R.; Desai, B.B. *Postharvest Biotechnology of Flowers and Ornamental Plants*; Springer Science & Business Media: Berlin/Heidelberg, Germany, 2012.
52. Liu, Z.; Luo, Y.; Liao, W. Postharvest physiology of fresh-cut flowers. In *Oxygen, Nitrogen and Sulfur Species in Post-Harvest Physiology of Horticultural Crops*; Elsevier: Amsterdam, The Netherlands, 2024; pp. 23–42.
53. Reid, M.S.; Jiang, C.Z. Postharvest biology and technology of cut flowers and potted plants. *Hortic. Rev.* **2012**, *40*, 3–56.
54. Finger, F.L.; Silva, T.P.; Araujo, F.F.; Barbosa, J.G. Postharvest quality of ornamental plants. In *Postharvest Ripening Physiology of Crops: Innovations in Postharvest Technology Series*; CRC Press: Boca Raton, FL, USA, 2016; p. 88.
55. Cheok, C.Y.; Ragunathan, A. Anthocyanin Degradation Kinetics and Thermodynamic Analysis of *Hibiscus Rosa-sinensis* L. *Clitoria ternatea* L. and *Hibiscus sabdariffa* L. *Prog. Energy Environ.* **2022**, 19, 1–12.
56. Tuly, S.S.; Mahiuddin, M.; Karim, A. Mathematical modeling of nutritional, color, texture, and microbial activity changes in fruit and vegetables during drying: A critical review. *Crit. Rev. Food Sci. Nutr.* **2023**, *63*, 1877–1900.
57. Pavan, M.A. Effects of Freeze Drying, Refractance Window Drying and Hot-Air Drying on the Quality Parameters of Açaí. Ph.D. Thesis, University of Illinois at Urbana-Champaign, Champaign, IL, USA, 2010.
58. van Doorn, W.G. Is petal senescence due to sugar starvation? *Plant Physiol.* **2004**, *134*, 35–42. [CrossRef]

Disclaimer/Publisher's Note: The statements, opinions and data contained in all publications are solely those of the individual author(s) and contributor(s) and not of MDPI and/or the editor(s). MDPI and/or the editor(s) disclaim responsibility for any injury to people or property resulting from any ideas, methods, instructions or products referred to in the content.